Karagozian & Case, Inc.

700 N. Brand Blvd., Suite 700

Glendale, CA 91203-3215

818-240-1919

www.kcse.com

*TR-19-35.1*

# HIGH-FIDELITY PHYSICS-BASED MODELING OF CROSS-LAMINATED TIMBER

Mark K. Weaver, S.E.
Shengrui Lan, Ph.D.

Prepared for:

Bill Parsons
Vice President of Operations
WoodWorks

October 9, 2020

The work upon which this publication is based was funded in part through a grant awarded by the FPL Coalition for Advanced Wood Structures. (Award number "17-JV-11111133-02")

**WoodWorks – Wood Products Council** provides education and free technical support related to the design, engineering and construction of commercial and multi-family wood buildings in the U.S. A non-profit organization staffed with architects, structural engineers and construction experts, WoodWorks has the expertise to assist with all aspects of wood building design, including (but not limited to): allowable heights and areas/construction types, structural detailing of wood and hybrid systems, fire resistance and acoustical-rated assemblies, efficient and code-compliant lateral system design, alternate means of code compliance, and energy-efficient detailing. For assistance with a project, visit www.woodworks.org/project-assistance or email help@woodworks.org. Visit our website at www.woodworks.org.

# EXECUTIVE SUMMARY


A series of high-fidelity physics-based (HFPB) calculations pertaining to the blast response of cross-laminated timber (CLT) panels are described herein. The primary objective of this HFPB modeling effort was to assess the ability of a continuum finite element approach to model CLT panels under complex quasi-static and dynamic (i.e., those associated with explosions) loading conditions. Panel responses both prior to and following rupture were considered. The modeling approach aimed to include the necessary fidelity to capture complex stress states explicitly while remaining feasible from a computational cost perspective.

Due to its anisotropic nature, wood is a difficult material to model in the HFPB context. An available material model developed by the FHWA (i.e., LS-DYNA’s MAT_143) was utilized in this effort on account of its wood-centric focus. This material model uses transversely isotropic constitutive equations and the Modified Hanshin yield criterion to track and simulate different post-peak behaviors exhibited by wood for different states of stress. It also considers rate effects by increasing material strength with increasing strain rate.

Material model fits for the lumber constituting Grades E1, V1, and V4 CLT were derived based on information provided in APA product reports. A series of single element simulations were performed to test these fits in compression, tension, and shear force paths. In general, the single element simulations reproduced the specified material properties. However, several areas requiring further investigation were identified:

- Beyond the proportional limit in compression, the MAT_143 material model response is essentially plastic. No softening in the compression parallel to grain response is apparent even though softening has been reported in the literature.

- Elements appear to exhibit a significant amount of deformation capability in shear beyond the proportional limit using the MAT_143 material model, which is different than the data (albeit limited in quantity) documented in the literature.

- An anomalous result observed while performing mesh size sensitivity studies leads to questions concerning the robustness of the mesh regularization scheme.

- The strength increases associated with strain rates ranging from 0.05 to 5 $s^{-1}$ (i.e., common strain rates for structural components exposed to blast loads) appear to be excessively high and have no parallel to other materials documented in the literature.

Using these material model fits, HFPB models of CLT panels without an in-plane axial load were subjected to a uniformly applied transverse quasi-static load in their major strength direction. To capture the observed failure at points of panel weakness (i.e., finger joints, knots), individual boards and finger joint locations were modeled. Sensitivity studies to ascertain optimal integration method type, mesh size, and loading rate were performed. The results of these simulations indicated that the generated material model fit well reproduced the initial stiffness, peak strength, and residual capacity of the panels in major strength direction bending.

Finally, quasi-static bending of biaxially-loaded CLT panels and dynamic bending of CLT panels were modeled using the developed material model fits and CLT panel modeling approach. These simulations uncovered several questions that suggest further investigation is required:

- The imposition of axial stress in combination with bending stress yielded computed peak panel strengths that were markedly less than those measured during testing. Thus, it is possible that the yield surface for biaxial stress states offered by MAT_143 underestimates the actual panel strength in bending. While a lower panel bending strength may lead to an overestimated peak deflection in bending, of more serious concern is that this may lead to the shear demand in the panel being underestimated.

- Applying blast loads to HFPB models of CLT panels produced markedly larger deflections than those measured in the test. Despite these large deflections, no panel rupture (or even attainment of the peak tension stress parallel to grain) was observed in the HFPB model even though significant panel rupture was observed in testing. This result is confusing, especially considering that the single element simulations did not exhibit a decrease in material stiffness with increasing strain rate, and that rupture was observed in quasi-static simulations of a similar nature (i.e., bending in the major strength direction).

# TABLE OF CONTENTS

# LIST OF FIGURES

## LIST OF TABLES

# LIST OF ACRONYMS

| | |
|---|---|
| AFB | Air Force Base |
| AFCEC | Air Force Civil Engineering Center |
| APA | The Engineered Wood Association |
| ASD | Allowable Stress Design |
| CLT | Cross-Laminated Timber |
| DFL | Douglas fir-Larch |
| DG | Displacement Gage |
| DIF | Dynamic Increase Factor |
| FE | Finite Element |
| HFPB | High-Fidelity Physics-Based |
| K-B | Kingery-Bulmash |
| LBE | Load Blast Enhanced |
| NDS | National Design Specification for Wood Construction |
| NLT | Nail-Laminated Timber |
| RP | Reflected Pressure Gage |
| SIF | Static Increase Factor |
| S-P-F | Spruce-Pine-Fir |
| STS | Self-Tapping Screws |
| UMaine | University of Maine |

# CHAPTER 1

# INTRODUCTION

As part of a Forest Products Laboratory Coalition for Advanced Wood Structures Grant, WoodWorks, Karagozian and Case, Inc. (K&C), and the Air Force Civil Engineer Center (AFCEC) partnered via a Cooperative Research and Development Agreement to extend the Phase 1 work described in Ref. [1, 2] as part of a follow-on Phase 2 effort. The overarching objectives of the Phase 2 effort were to demonstrate:

- the ability of loaded cross-laminated timber (CLT) construction to resist blast loads generated by high explosives and still be able to support their tributary service load; and

- the ability of different mass timber configurations to resist blast loads generated by high explosives. The mass timber configurations considered included: (1) 5-ply CLT panels, (2) alternative connection configurations that utilized pre-fabricated brackets and self-tapping screws, and (3) nail-laminated timber (NLT) panels.

To fulfill these objectives, two distinct series of tests were performed as part of the Phase 2 effort:

- Twenty-four quasi-static laboratory tests were used to investigate the out-of-plane bending response of axially-loaded CLT panels in their major strength direction under a uniformly-applied transverse quasi-static load. These tests varied the applied axial load, CLT grade, number of panel plies, and panel length.

- Four arena blast tests were performed on three full-scale CLT structures. The first two tests were used to demonstrate the ability of axially-loaded CLT panels to resist blast loads while the second two tests were used to demonstrate the ability of different mass timber configurations to resist blast loads. In both test series, the first shot was intended to keep the panels elastic and the second shot was intended to rupture panels. Ruptured panels were removed and replaced prior to performing the first test in each series.

The technical approach, test setup, results obtained, and conclusions generated from these Phase 2 tests are documented in Ref. [3].

Following the conclusion of these Phase 2 tests, a series of high-fidelity physics-based (HFPB) calculations of various tests executed in the Phase 1 and 2 efforts were performed. Of interest was to investigate how effectively HFPB calculations could be used to learn more about the complex states of stress and failures observed in the quasi-static load tree and arena blast tests. To generate the material model fit used in these calculations, a selection of the quasi-static tests performed at the University of Maine (UMaine) in Phase 1 were modeled as well. This report documents this HFPB modeling work, highlights applications for this type of analysis, and indicates areas where further effort is needed to enhance the described modeling approach.

## 1.1 BACKGROUND

In a structural response context, an HFPB model is a broad term used to describe an analytical model that is designed to simulate the actual behavior exhibited by a structure, usually exposed to some form of extreme loading. These models generally employ many degrees of freedom in order to solve the foundational equation of classical mechanics, Newton's second law of motion. In this report, the HFPB model utilized is based on a macroscale continuum finite element (FE) framework, although HFPB models could be based on other analytical formulations (e.g., meshfree) and use different scales (e.g., meso, micro) as well. The utilization of HFPB models allows for the explicit modeling of important behaviors essential to capturing nonlinear structural responses resulting from the application of fast transient loads (i.e., those associated with explosions). Some of these behaviors include:

- Material nonlinearity and geometric nonlinearity (i.e., large deformation response).
- Material strength increases associated with increasing strain rate.
- Structural three-dimensional behavior with complex and time-variant stress states (i.e., not only flexural but also axial, shear and torsional stresses in combination).
- Structural response simultaneously at both the global and local (e.g., at connections) levels.
- Blast loads applied with different arrival times and pressure histories at different locations (i.e., non-uniform loading).
- Contact interfaces to consider load transfer from structural elements that collide during the simulation.
- Realistic boundary conditions that account for the partial fixity at support points.

## 1.2 OBJECTIVE

The primary objective of this effort was to assess the ability of a continuum FE approach to model CLT panels under complex quasi-static and dynamic loading conditions (e.g., those associated with explosions). Panel response both prior to and following rupture was considered. The developed model aimed to include the necessary fidelity to capture complex stress states explicitly while still being feasible from a computational cost perspective. Thus, a macroscale modeling approach was adopted. Test data obtained via the Phase 1 [1, 2] and 2 [3] efforts was used to evaluate the efficacy of the developed model. Several specific goals were identified and used to guide this effort from its outset:

- To document the analytical assumptions used to construct FE meshes of CLT panels using continuum elements.
- To document the process by which a fit can be generated for LS-DYNA Material Model 143 to include post-peak response.

- To compare results generated by these HFPB modeling techniques with quasi-static and blast test data.

## 1.3 REPORT OUTLINE

The remainder of this report is divided into five chapters:

- Chapter 2 describes the process used to generate a material model fit for CLT. LS-DYNA Material Model 143 (i.e., MAT_143) was selected for this. Included in this chapter are the results of a series of single-element studies performed to investigate this material model's capabilities.

- Chapter 3 documents the results of a series of HFPB analyses performed to model the quasi-static panel tests performed at the University of Maine in Phase 1 [1].

- Chapter 4 uses the material model fits documented in Chapter 2 to assess MAT_143's ability to model the quasi-static tests that exposed CLT panels to both axial and out-of-plane loads simultaneously performed at AFCEC in Phase 2 [3].

- Chapter 5 uses the material model fits documented in Chapter 2 to assess MAT_143's ability to model the Grade E1 CLT structure during blast Tests 2, 3, and 7 performed in Phases 1 and 2 at Tyndall AFB [2, 3].

- Chapter 6 presents general conclusions made as a result of the analyses described herein.

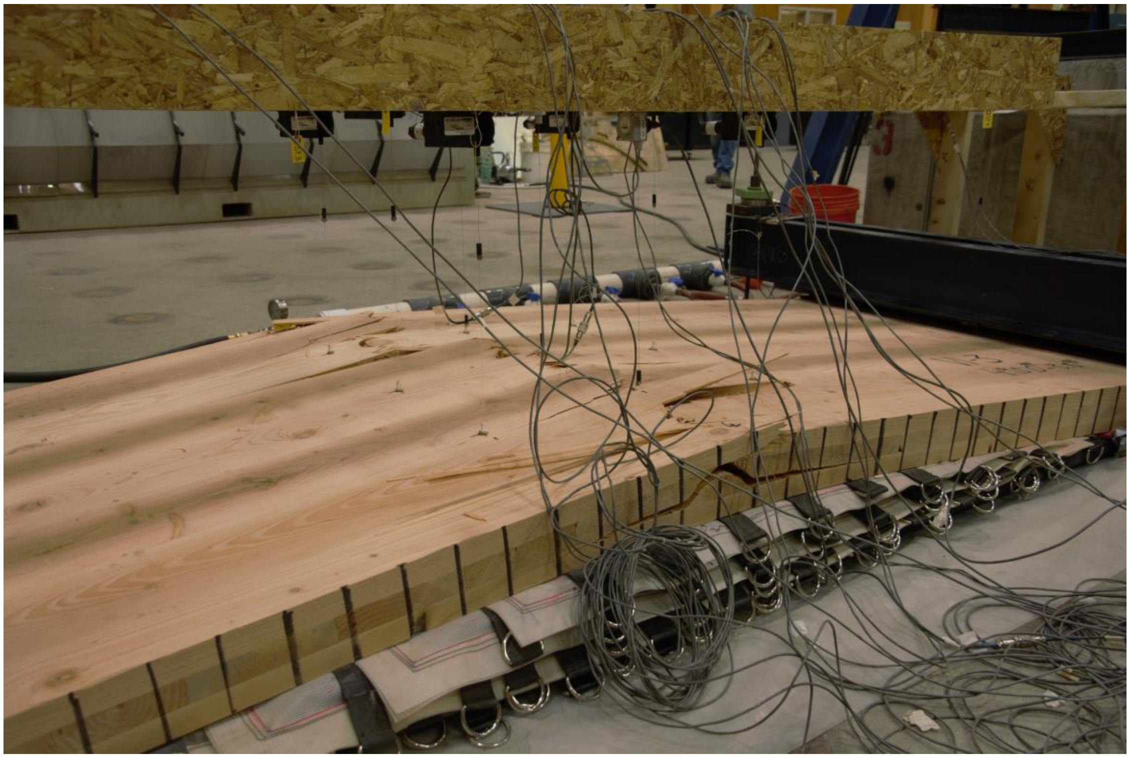

*(a) Quasi-static panel test without axial load performed at UMaine.*

**Figure 1-1. Photographs of Phases 1 and 2 Testing.**

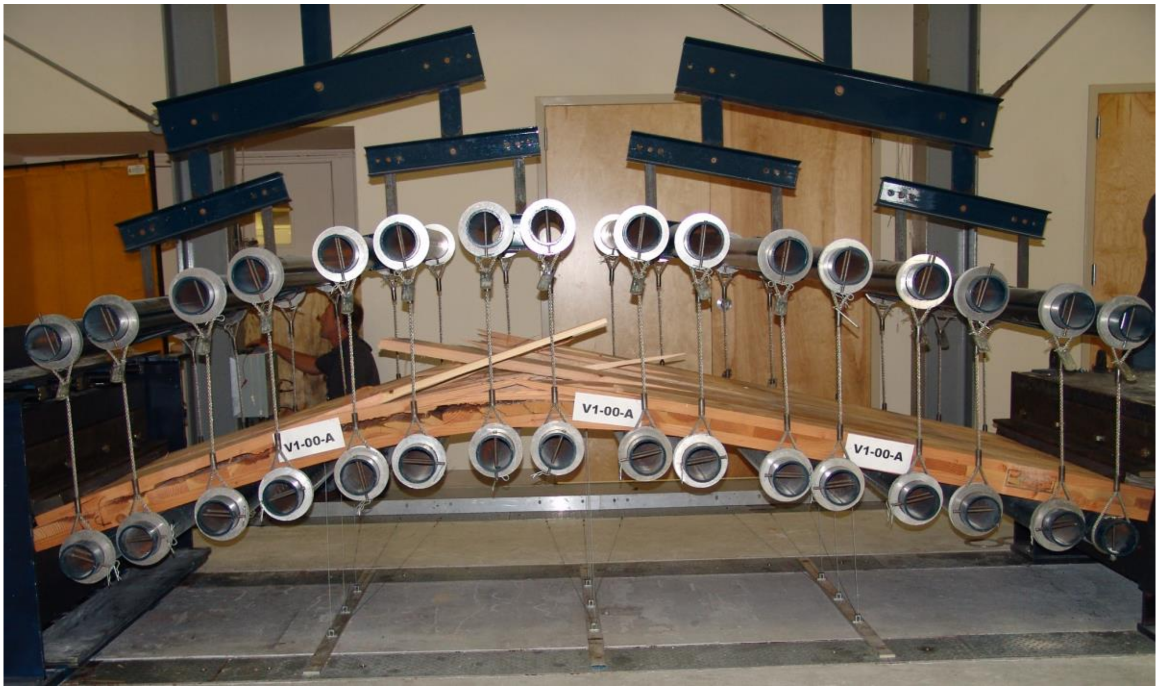

*(b) Quasi-static panel test with axial load performed at AFCEC.*

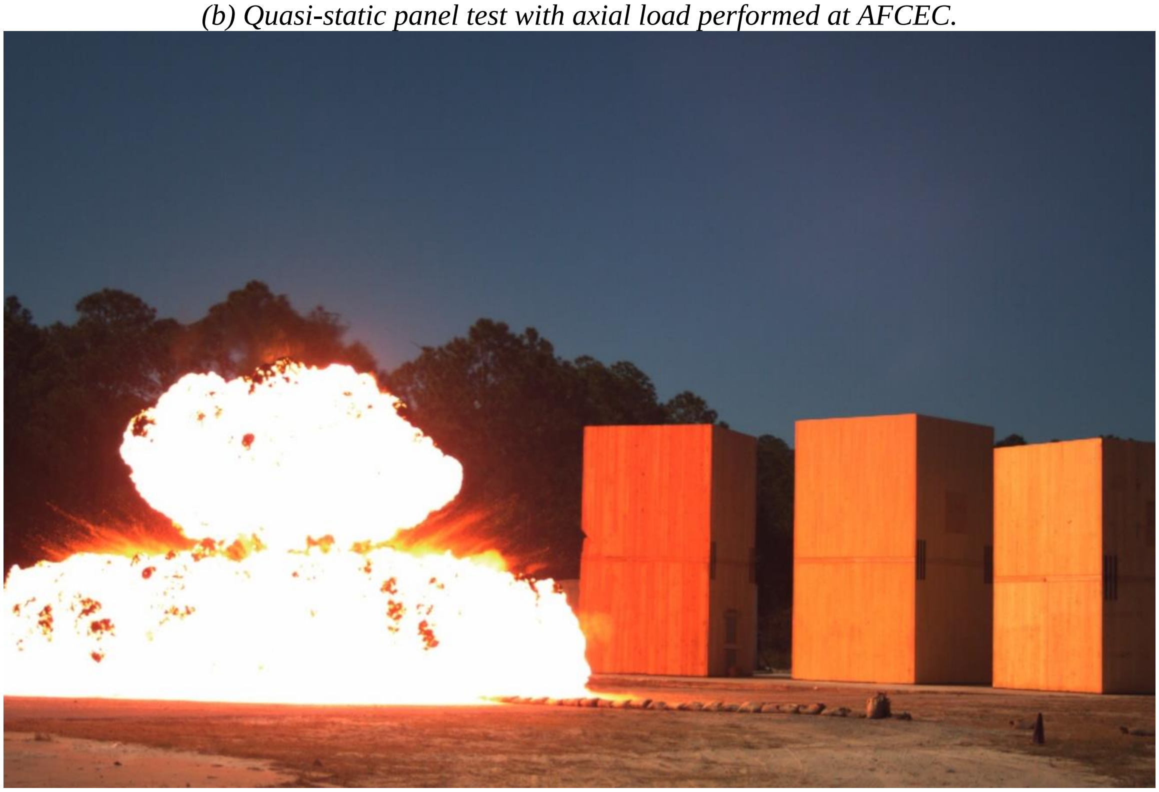
*(c) Blast Test 3 performed at Tyndall AFB.*

**Figure 1-1. Photographs of Phases 1 and 2 Testing. (Cont'd)**

# CHAPTER 2

# MATERIAL MODEL FIT GENERATION

This chapter describes how the MAT_143 material model in LS-DYNA can be fit specifically to model the behavior of a generic CLT panel. The chapter opens with a brief description of MAT_143 and its capabilities. Section 2.2 then describes the various parameters that a user needs to fit the MAT_143 material model and how to obtain these values for a generic CLT. Both the major and minor strength directions of the panel are considered. Finally, Section 2.3 documents a series of single-element studies performed to confirm that the fit performs as expected.

## 2.1 WOOD MATERIAL RESPONSE SYNOPSIS

Wood presents a unique material model challenge. Whereas many materials are idealized as isotropic (e.g., steel, concrete) at the macroscale for the purposes of analysis, the fibrous nature of wood is characteristically anisotropic. However, for simplicity, wood is commonly idealized as an orthotropic material according to the longitudinal, tangential, and radial directions illustrated in Figure 2-1.

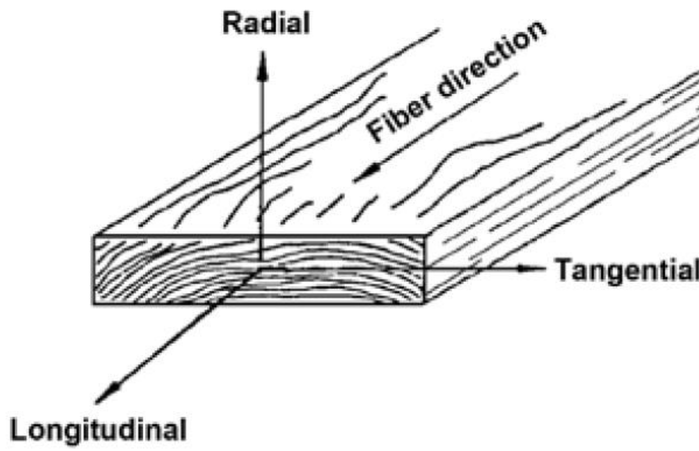


**Figure 2-1. Fiber Directions in Wood [4].**

While the tangential and radial directions have similar material properties, and thus are often idealized with the same material properties in analysis, the longitudinal direction has vastly different properties. Thus, a transversely isotropic material model is necessary (at a minimum) to explicitly capture wood structural response at the macroscale. The longitudinal direction is often referred to as the “parallel” direction and the tangential and radial directions are referred to as “perpendicular” directions.

The macro response of wood prior to peak strength is well idealized by the elastic constitutive equations for an orthotropic material [4]. However, the post-peak response of wood varies significantly based on the stress state (i.e., combinations of stresses) that may eventuate in failure. Figure 2-2 illustrates this phenomenon for uniaxial tension and compression stress paths. As shown, tension stress in the longitudinal (L) direction leads to a sharp sudden loss of stress following material rupture. In contrast, the post-peak response in compression is marked by a semblance of ductility in all three directions. It should also be noted that the magnitude of the peak compressive stress in the longitudinal (i.e., parallel) direction is characteristically larger than that in the tangential (T) or radial (R) (i.e., perpendicular) directions.

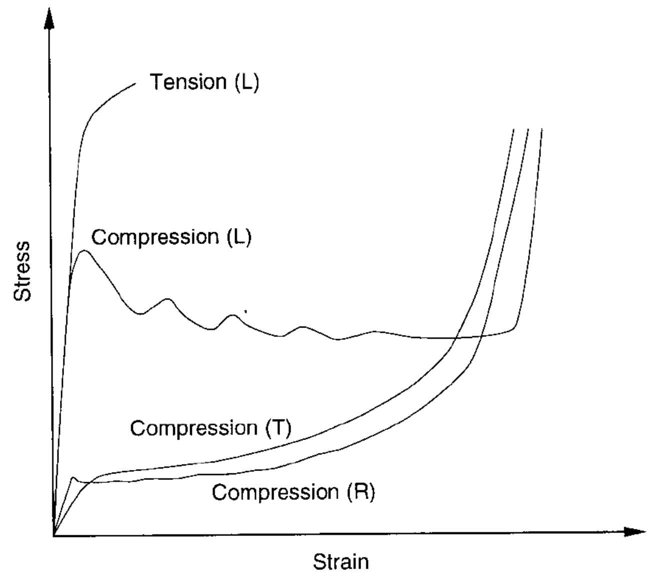


**Figure 2-2. Idealized Stress-Strain Curves for Wood [5].**
*(Shown for 3 fiber directions: L = longitudinal, T= tangential, and R = radial)*

The presence of confinement can substantially influence the post-peak response of wood in compression as illustrated in Figure 2-3. This is shown in the behavior for spruce wood in both the parallel and perpendicular to grain directions. When compressive load is applied in the parallel to grain direction (Figure 2-3a), the presence of confinement (i.e., lateral dilatation constrained) limits the post-peak softening exhibited by the wood. In contrast, the presence of confinement does not markedly impact the nature of the post-peak response of the wood in the perpendicular to grain direction (Figure 2-3b).

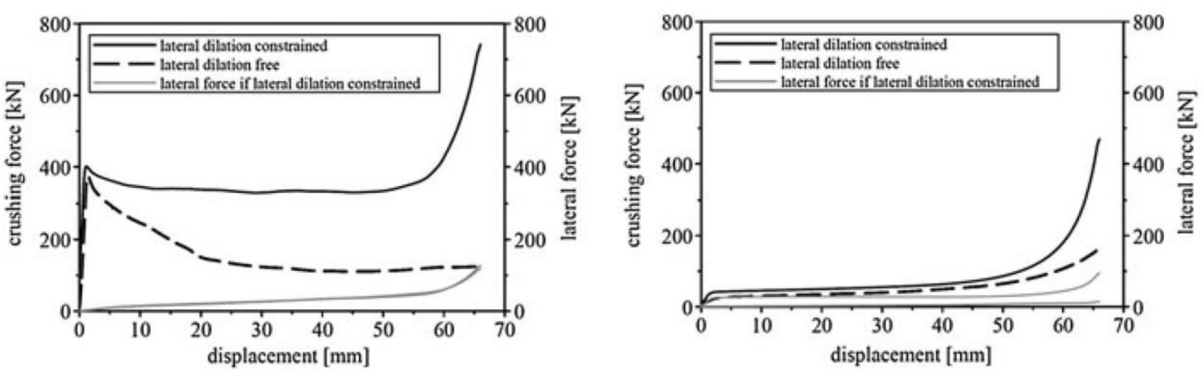


*(a) Parallel to Grain Direction.* *(b) Perpendicular to Grain Direction.*
**Figure 2-3. Effect of Confinement on Post-Peak Compressive Response of Spruce [6].**

The post-peak response of wood in shear is generally termed brittle, although the amount of deformation prior to rupture once the proportional limit is reached appears to vary based on the limited information documented in the literature. For example, very limited shear deformation following the proportional limit was reported for larch wood (Figure 2-4a) whereas much larger plastic deformations were reported for pine when sheared in the longitudinal-tangential plane (Figure 2-4b). This testing on pine also indicated relative weakness of wood sheared in the radial-tangential plane as compared to either the longitudinal-tangential or longitudinal-radial planes (Figure 2-4b and c). This radial-tangential (i.e., “rolling”) shear strength of wood is important when attempting to identify the out-of-plane resistance of CLT panels.

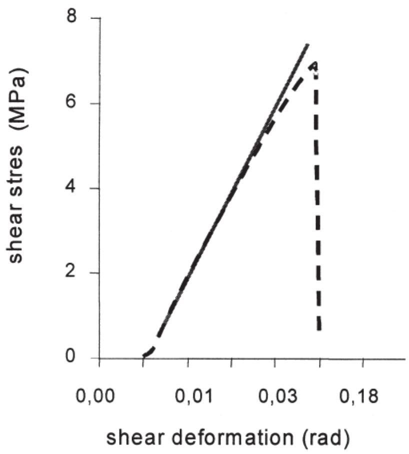


*(a) Larch (unknown plane)* [7].

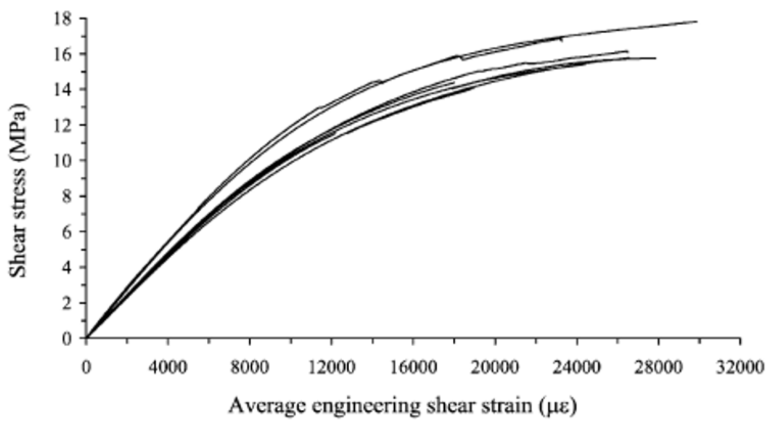


*(b) Pine (LT plane)* [8].

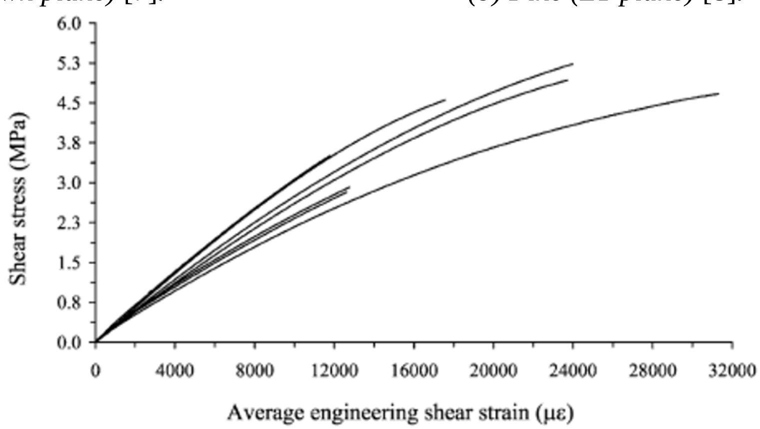


*(c) Pine (RT plane)* [8].

**Figure 2-4. Post-Peak Shear Response of Different Types of Wood.**

In addition to material anisotropy, wood material responses are further complicated by environmental conditions. Of primary importance is the dependence of wood stiffness and strength on its moisture content. Figure 2-5 illustrates this dependence for clear wood for bending modulus of elasticity, modulus of rupture, and maximum compressive strength parallel to grain. In general, increasing moisture content decreases both the strength and stiffness properties of wood. For the testing performed in Phases 1 and 2, the moisture content of the CLT panels was relatively constant (i.e., 12% ± 3%).

Another notable consideration is the short durations of blast-load-induced response. Wood material strengths have been shown to exponentially increase with increasing strain rate [9]. The National Design Specification (NDS) includes a load duration factor, $C_D$, to account for this phenomenon [10]. There is limited publicly available test data that explicitly characterizes wood materials at strain rate levels consistent with blast loads (i.e., between 0.1 and 10 $s^{-1}$). Available test data generally concentrates on either higher strain rates through use of the split Hopkinson pressure bar [11, 12] or lower strain rates (e.g. [13]).

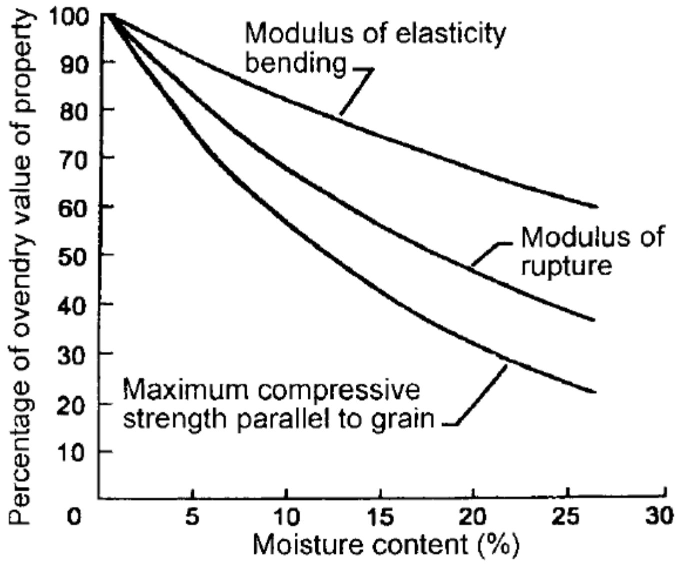


**Figure 2-5. Effect of Moisture Content on Clear Wood Properties [14].**

## 2.2 HFPB ANALYSIS OVERVIEW

This effort concentrated on modeling CLT panels with a continuum finite element model. The multi-physics solver LS-DYNA was the analysis code used to generate the models. The MAT_143 material model was employed to approximate the wood's behavior. Both single point and selective reduced integration of the continuum element were investigated.

### *2.2.1 Finite Element Solver*

LS-DYNA is an advanced general-purpose multi-physics code that is widely used by the blast and impact effects analysis community. Originally developed at Lawrence Livermore National Laboratory in the 1970s, the code is well suited to address highly nonlinear transient structural response problems through its explicit time integration solver. Release 10.0 of LS-DYNA was utilized to perform the analyses reported herein. More information on the features and capabilities of LS-DYNA can be found in [15].

### *2.2.2 Material Model*

A material model that is transversely isotropic is supported by Release 10.0 of LS-DYNA. This material model (i.e., MAT_143) was developed through funding provided by the Federal Highway Administration (FHWA). Several features of this material model that make it suited to analyze wood for both quasi-static and dynamic loads include:

- transversely isotropic constitutive equations;

- yield surfaces based on the Modified Hanshin criterion with plastic flow;
- pre-peak and late-time hardening;
- damage-based softening with erosion;
- automatic mesh regularization; and
- rate effects for high-strain rate applications.

A manual that describes the theory undergirding the above features is publicly-available [16]. In addition, a series of validation exercises are formally documented in [17].

## 2.3 MATERIAL MODEL FIT

A list of the input parameters needed to generate a fit for MAT_143 are included in Table 2-1. This section provides input on how to obtain each of these parameters and the basis for their determination.

All of the information needed to fill out of the parameters needed for the MAT_143 material card can be derived from information included in the APA product report. Several APA product reports for CLT manufacturers in the U.S. include Ref. [18, 19, 20, 21]. The information that is most pertinent to deriving the material model fit can be found in the "ASD Reference Design Value" table included within these reports. An example of this data pulled from [19] is included in Figure 2-6.

Table 1. ASD Reference Design Values[(a)] for Lumber Laminations Used in SmartLam CLT (for Use in the U.S.)

| CLT Grade | Laminations Used in Major Strength Direction | | | | | | Laminations Used in Minor Strength Direction | | | | | |
|---|---|---|---|---|---|---|---|---|---|---|---|---|
| | $F_b$ (psi) | E ($10^6$ psi) | $F_t$ (psi) | $F_c$ (psi) | $F_v$ (psi) | $F_s$ (psi) | $F_b$ (psi) | E ($10^6$ psi) | $F_t$ (psi) | $F_c$ (psi) | $F_v$ (psi) | $F_s$ (psi) |
| SL-V4 | 775 | 1.1 | 350 | 1,000 | 135 | 45 | 775 | 1.1 | 350 | 1,000 | 135 | 45 |

For SI: 1 psi = 0.006895 MPa

(a) Tabulated values are allowable design values and not permitted to be increased for the lumber flat use or size factor in accordance with the NDS. The design values shall be used in conjunction with the section properties provided by the CLT manufacturer based on the actual layup used in manufacturing the CLT panel (see Tables 2 and 3).

**Figure 2-6. Example of ASD Reference Design Value Table from APA Product Report.**

It is important to note that the values listed in the APA product report are allowable stress design (ASD) properties, which are based on 5$^{th}$ percentile material properties. Actual, or 50$^{th}$ percentile, strength values are necessary when performing HFPB modeling. A method to transform these 5$^{th}$ percentile to 50$^{th}$ percentile values is discussed in depth in Appendix B of PDC-TR 18-02 [22]. Pertinent information from this technical report as it relates to generating the material model fit is mentioned herein.

**Table 2-1. MAT_143 Parameters.**

| Parameter ID | Parameter Description | Parameter Group | Report Section |
|---|---|---|---|
| RO | Mass density | Density / Stiffness | 0 |
| EL | Parallel normal modulus | | |
| ET | Perpendicular normal modulus | | |
| GLT | Parallel shear modulus | | |
| GTR | Perpendicular shear modulus | | |
| PR | Parallel major Poisson's ratio | | |
| XT | Parallel tensile strength | Strength | 2.3.2 |
| XC | Parallel compressive strength | | |
| YT | Perpendicular tensile strength | | |
| YC | Perpendicular compressive strength | | |
| SXY | Parallel shear strength | | |
| SYZ | Perpendicular shear strength | | |
| GF1∥ | Parallel fracture energy in tension | Damage | 2.3.3 |
| GF2∥ | Parallel fracture energy in shear | | |
| BFIT | Parallel softening parameter | | |
| DMAX∥ | Parallel maximum damage | | |
| GF1⊥ | Perpendicular fracture energy in tension | | |
| GF2⊥ | Perpendicular fracture energy in shear | | |
| DFIT | Perpendicular softening parameter | | |
| DMAX⊥ | Perpendicular maximum damage | | |
| FLPAR | Parallel fluidity parameter for tension & shear | Rate Effects | 2.3.4 |
| FLPARC | Parallel fluidity parameter for compression | | |
| POWPAR | Parallel power | | |
| FLPER | Perpendicular fluidity parameter for tension & shear | | |
| FLPERC | Perpendicular fluidity parameter for compression | | |
| POWPER | Perpendicular power | | |
| NPAR | Parallel hardening initiation | Hardening | 2.3.5 |
| CPAR | Parallel hardening rate | | |
| NPER | Perpendicular hardening initiation | | |
| CPER | Perpendicular hardening rate | | |

### 2.3.1 Density and Stiffness Parameters

The density and stiffness parameters for MAT_143 shown in Table 2-1 are defined in this section. The mass density (*RO*) can be defined according to Equation (1):

$$RO = \left(1 + \frac{MC}{100}\right) * SG * \rho_W \tag{1}$$

where:

*MC* = Moisture content percentage. In the absence of further information, moisture content percentage can be assumed to be 12 percent; see Section 6.1.4 of [23].

*SG* = Specific gravity. Values for many species are included in Table 12.3.3A of [10].

$\rho_W$ = Mass density of water.

The parallel (to grain) normal modulus (*EL*) is simply the modulus of elasticity, *E*, defined in the applicable APA product report for the applicable strength direction (i.e., major or minor; see Figure 2-6). The perpendicular (to grain) normal modulus (*ET*), parallel shear modulus (*GLT*), and perpendicular shear modulus (*GTR*) can be defined according to Equations (2), (3), and (4), respectively:

$$ET = \frac{EL}{45} \tag{2}$$

$$GLT = \frac{EL}{16} \tag{3}$$

$$GTR = \frac{GLT}{10} \tag{4}$$

These definitions of *GLT* and *GTR* are based on footnote "d" of Table A1 in PRG 320 [23]. Concerning *ET*, this same footnote states that when calculating CLT design properties, the transverse *E* (i.e., *ET*) should be assumed to be *EL*/30. The PRG 320 properties, however, are incompatible with those used in MAT_143 in LS-DYNA, which requires that *ET* be less than four times the magnitude of *GTR* (i.e., *ET* would have to be less than *EL*/40). Figure 2-7 shows the error message returned if this is not the case. Given the fact that both conditions cannot hold simultaneously and the importance of capturing the "rolling" shear stiffness when computing panel response in the major strength direction, for the analyses described herein the value for *ET* was set equal to *EL*/45 rather than increasing *GTR*.

```
*** Warning 20177 (STR+177)
    *MAT_WOOD for part number 3
    The perpendicular normal modulus (ET) must be less than 4
    times the magnitude of the perpendicular shear modulus (GTR)
```

**Figure 2-7. MAT_143 Error Message Related to *ET* and *GTR*.**

The parallel major Poisson's ratio (*PR*) can be defined by averaging values provided in Table 5-2 of the FPL *Wood Handbook* [4]. In this table values for $\mu_{LR}$ (i.e., Poisson's ratio for deformation along the radial axis caused by stress along the longitudinal axis) and $\mu_{LT}$ (i.e., Poisson's ratio for deformation along the tangential axis caused by stress along the longitudinal axis) are given, which were averaged to obtain the *PR* value used in MAT_143.

In many cases, the NDS species designation (e.g., Spruce-Pine-Fir) is an amalgamation of several species noted in this table (i.e., as defined in Table 6-7 of the FPL *Wood Handbook*). Where this is the case, *PR* is averaged across the species noted in Table 6-7 of the FPL *Wood Handbook.*

### 2.3.2 Strength Parameters

The parallel tensile strength (*XT*), parallel compressive strength (*XC*), perpendicular compressive strength (*YC*), parallel shear strength (*SXY*), and perpendicular shear strength (*SYZ*) can be defined according to Equations (5), (6), (7), (8), and (9), respectively:

$$XT = SIF_b * DIF * F_t \tag{5}$$

$$XC = SIF_c * DIF * F_c \tag{6}$$

$$YC = SIF_{c\perp} * DIF * F_{c\perp} \tag{7}$$

$$SXY = SIF_s * DIF * F_v \tag{8}$$

$$SYZ = SIF_s * DIF * F_s \tag{9}$$

where:

$SIF_b$ = Static increase factor (SIF) for flatwise bending (based on wood species and effective depth of member; see Section 7.2 of PDC-TR 18-02 [22]).

$SIF_c$ = SIF for compression parallel to grain (= 1.68; see Section 7.2 of PDC-TR 18-02).

$SIF_{c\perp}$ = SIF for compression perpendicular to grain (= 1.68; see Section 7.2 of PDC-TR 18-02. It could be argued that this value severely underestimates the SIF for compression stress perpendicular to grain. Using the process described in Appendix C of PDC-TR 18-02, this SIF could be as high as 3.10. The $K_{char}$, $K_{avg}$, and $K_{size}$ factors could be taken to be 1.67, 1.85, and 1.00, respectively. This $K_{char}$ factor is defined in Table 5 of ASTM D2915 [24] and this $K_{avg}$ factor is based on an assumed normal distribution and a 28-percent coefficient of variation (Table 5-6 of [4]) However, in light of the relatively limited amount of information concerning the actual compression strength of wood in the perpendicular to grain direction, it is recommended that the lower (i.e., 1.68) be used for now).

$SIF_s$ = SIF for flatwise shear (= 2.60; see Section 7.2 of PDC-TR 18-02).

| | | |
|---|---|---|
| $DIF$ | = | Dynamic increase factor (DIF) (see Section 2.3.4). |
| $F_t$ | = | ASD reference axial tensile stress defined in the applicable APA product report for the strength direction of concern (e.g., see Figure 2-6). |
| $F_c$ | = | ASD reference axial compressive stress parallel to grain defined in the applicable APA product report for the strength direction of concern (e.g., see Figure 2-6). |
| $F_{c\perp}$ | = | ASD reference axial compressive stress perpendicular to grain defined in NDS Supplement [25] for the strength direction of concern. |
| $F_v$ | = | ASD reference shear stress defined in the applicable APA product report for the strength direction of concern (e.g., see Figure 2-6). |
| $F_s$ | = | ASD reference planar (rolling) shear stress defined in the applicable APA product report for the strength direction of concern (e.g., see Figure 2-6). |

The perpendicular tensile strength (*YT*) can be defined according to Equation (10) for softwoods and Equation (11) for hardwoods:

$$YT = \frac{XT}{30} \tag{10}$$

$$YT = \frac{XT}{20} \tag{11}$$

The coefficients in the denominator in Equations (10) and (11) are based on material property data included in Table 5-3 of the *Wood Handbook* [4]. Specifically, the modulus of rupture was divided by the tension strength perpendicular to grain recorded for the species listed in this table. A total of 35 softwood and 44 hardwood species were considered. The computed ratios ranged from 22.4 to 52.5 with an average of 31.8 for the softwoods and from 13.4 to 32.2 with an average of 19.0 for the hardwoods. Additionally, [16] notes that “the parallel tensile strength of pine is 30 to 50 times greater than the perpendicular tensile strength”.

It should be noted that, preferably, the ratio would be tension strength parallel to grain (rather than modulus of rupture) divided by tension strength perpendicular to grain. Generally, a wood’s tension strength parallel to grain is less than its modulus of rupture. However, this data is not readily available for many species. Considering the relative complexity in measuring and variation inherent in the tension strength perpendicular to grain material property, the coefficients shown in Equations (10) and (11) are considered reasonable estimates.

### 2.3.3 Damage Parameters

Due to a lack of additional data, it was deemed reasonable that the default MAT_143 damage parameters be used. These damage parameters are shown in Table 2-2. More information concerning the derivation of these damage parameters can be found in [16].

**Table 2-2. Default MAT_143 Damage Parameters.**

| PARALLEL | | | | PERPENDICULAR | | | |
|---|---|---|---|---|---|---|---|
| BFIT | GF1∥ [psi-in] | GF2∥ [psi-in] | DMAX∥ | DFIT | GF1⊥ [psi-in] | GF2⊥ [psi-in] | DMAX⊥ |
| 30 | 128 | 479 | 0.9999 | 30 | 1.20 | 4.50 | 0.99 |

### 2.3.4 Rate Effects Parameters

For load durations of greater than one second, the applicable load duration factor, $C_D$, from the NDS be used as the DIF in Equations (5) through (9) was used. Performing simulations using explicit time integration for durations longer than 1 second is generally too computationally expensive. Care must be taken to disable rate effects in the material card.

For load durations less than one second, the DIF in Equations (5) through (9) were set equal to one. Due to the limited amount of test data documenting the response of wood at high strain rates, it was deemed reasonable to use the default MAT_143 rate effects parameters. These damage parameters are shown in Table 2-3. More information concerning the derivation of these damage parameters can be found in [16].

**Table 2-3. Default MAT_143 Rate Effects Parameters.**

| PARALLEL | | | PERPENDICULAR | | |
|---|---|---|---|---|---|
| FLPAR | FLPARC | POWPAR | FLPER | FLPERC | POWPER |
| 0.0045 | 0.0045 | 0.107 | 0.0962 | 0.0962 | 0.104 |

### 2.3.5 Hardening Parameters

Due to a lack of additional data, it was deemed reasonable that the default MAT_143 hardening parameters be used. These damage parameters are shown in Table 2-4. More information concerning the derivation of these damage parameters can be found in [16].

**Table 2-4. Default MAT_143 Hardening Parameters.**

| PARALLEL | | PERPENDICULAR | |
|---|---|---|---|
| NPAR | CPAR | NPER | CPER |
| 0.5 | 400 | 0.4 | 100 |

## 2.4 SINGLE ELEMENT STUDIES

A series of single element studies were performed to test the material model fit described in Section 2.3. Fits were created for the lumber comprising three grades of CLT:

- Grade E1 [18]: 1950f-1.7E Spruce-Pine-Fir (S-P-F) (major strength direction); No.3 S-P-F (minor strength direction)
- Grade V1 [20]: No.2 Douglas fir-Larch (DFL) (major strength direction); No.3 DFL (minor strength direction)
- Grade V4 [19]: No.2 S-P-F (South) (major and minor strength directions)

Stress path responses were investigated for compression (C), tension (T), and shear (V) load paths in both the parallel (||) and perpendicular (⊥) to grain directions. A 1-inch cube element was used as the default case. No confinement pressure in the off-axis directions was provided. Boundary conditions for the single element models for each force path were as follows:

- **Tension / Compression**: Nodes 1 through 4 (see Figure 2-8) were constrained in Z-translation.

- **Shear**: Nodes 1 through 8 were constrained in Z-translation and nodes 1 through 4 were also constrained in X-translation.

For the tension and compression stress path simulations, nodes 5 through 8 were moved at a constant velocity in the positive Z-direction and negative Z-direction, respectively. For the shear simulations, nodes 5 through 8 were moved at a constant velocity in the positive X-direction.

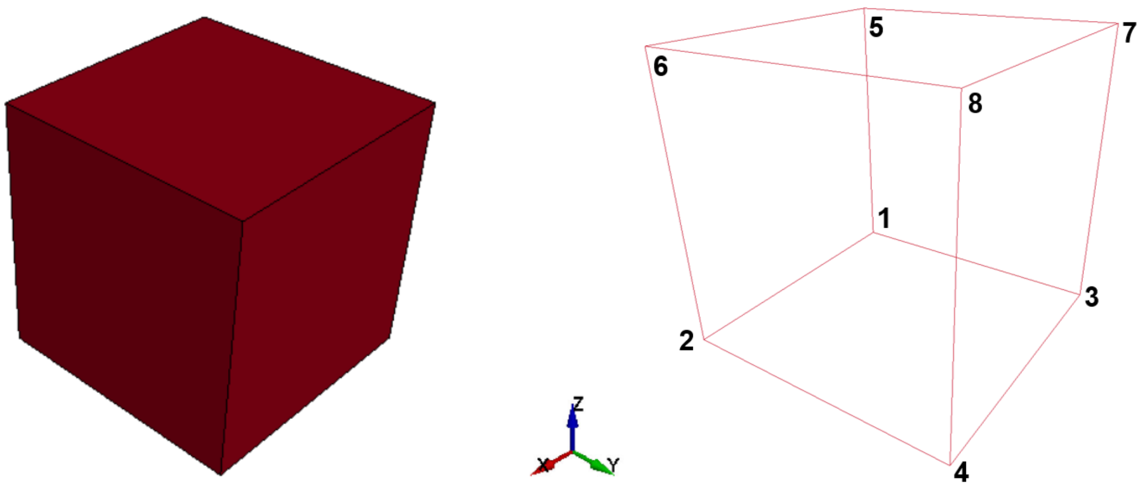


*(a) Isometric View.* *(b) Node IDs.*

**Figure 2-8. Single Element FE Model.**

Figure 2-9 through Figure 2-11 display the results of these single element studies for the Grade E1, Grade V1, and Grade V4 lumber, respectively. The stiffness and peak strengths defined by the fit are faithfully reproduced in the single element study results. However, two behaviors observed in these simulations appear to run counter to the wood material response phenomenology summarized in Section 2.1:

- Beyond the proportional limit in compression, the material response is essentially plastic. No softening in the compression parallel to grain response is apparent even though softening has been reported in the literature.

- The shear response beyond the proportional limit appears to exhibit a significant amount of plastic deformation, which is different than the data (albeit limited) documented in the literature.

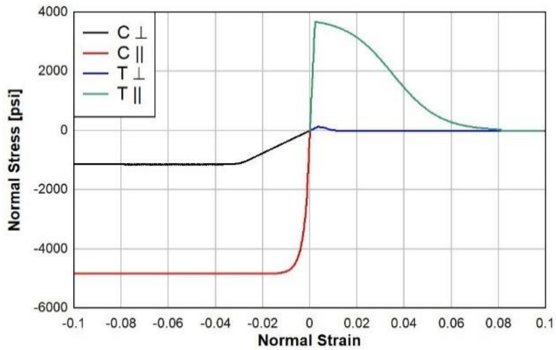


*(a) 1950f-1.7E S-P-F – Tension/Compression.*

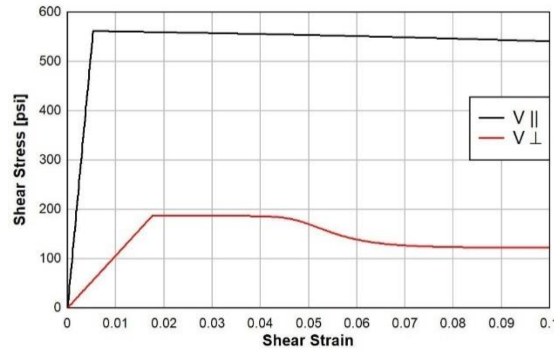


*(b) 1950f-1.7E S-P-F – Shear.*

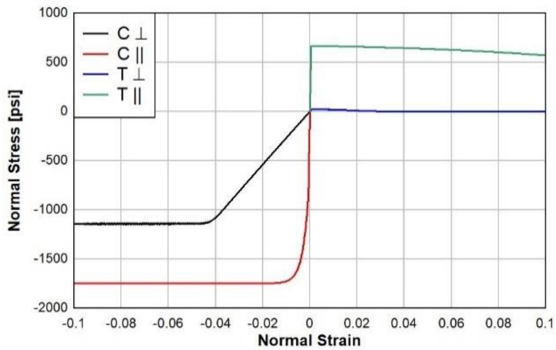


*(c) No.3 S-P-F – Tension/Compression.*

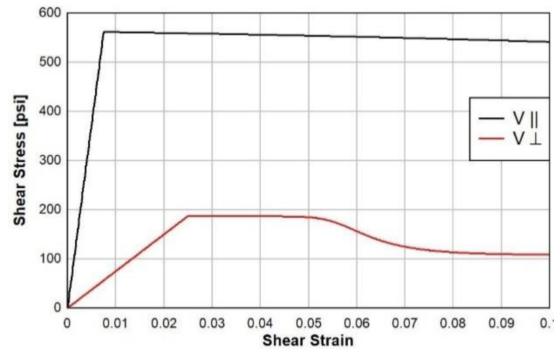


*(d) No.3 S-P-F – Shear.*

**Figure 2-9. Grade E1 Single Element Model Results.**

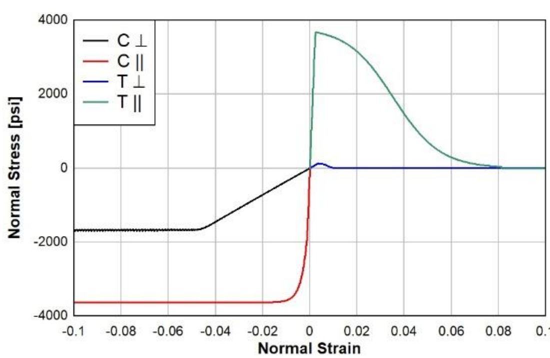


*(a) No.2 DFL – Tension/Compression.*

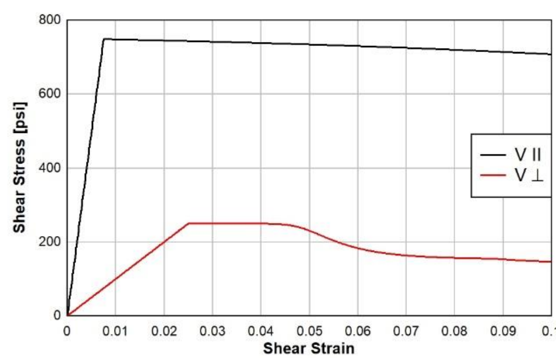


*(b) No.2 DFL – Shear.*

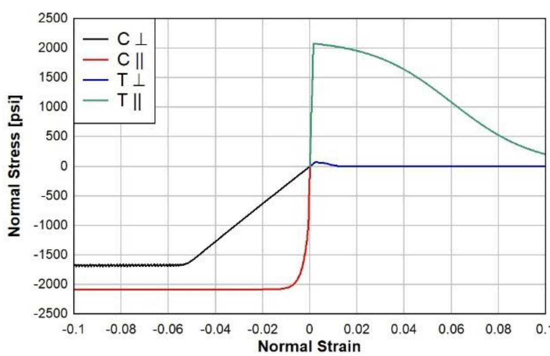


*(c) No.3 DFL – Tension/Compression.*

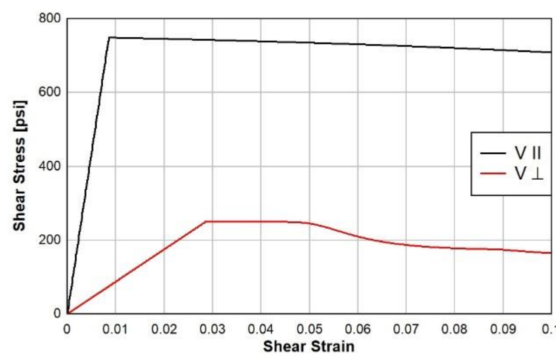


*(d) No.3 DFL – Shear.*

**Figure 2-10. Grade V1 Single Element Model Results.**

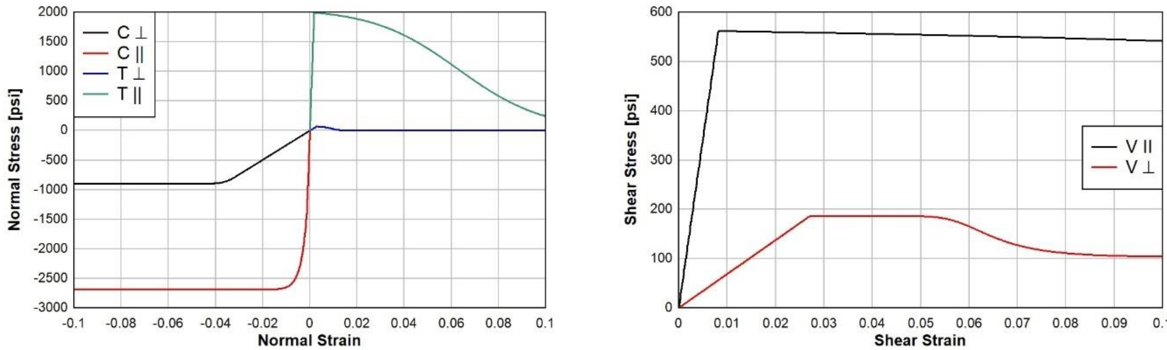


*(a) No.2 S-P-F (South) – Tension/Compression.* *(b) No.2 S-P-F (South) – Shear.*

**Figure 2-11. Grade V4 Single Element Model Results.**

Following these initial single element studies, two parametric studies were performed to investigate the capability of MAT_143. All additional studies were based on the Grade E1, major strength direction lumber (i.e., 1950f-1.7E S-P-F). The first parametric study was a mesh sensitivity study to investigate the mesh size impact on the post-peak response in the compression, tension, and shear load paths. Figure 2-12 documents the results of this mesh sensitivity study.

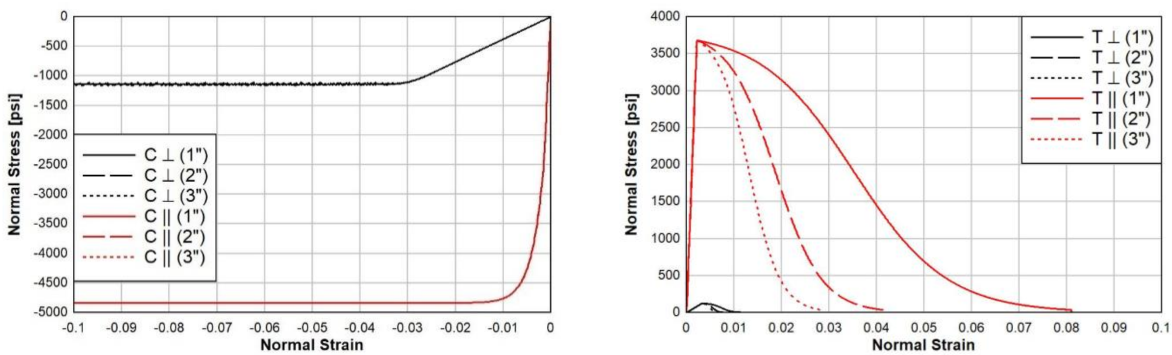


*(a) Compression.* *(b) Tension.*

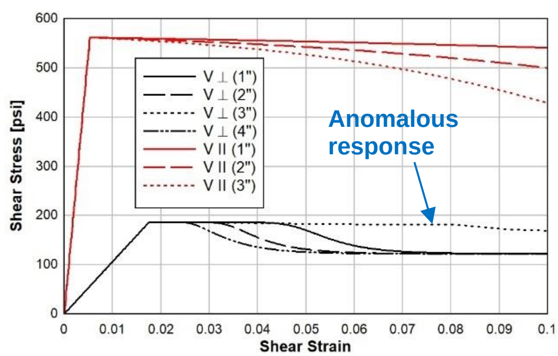


*(c) Shear.*

**Figure 2-12. Single-Element Mesh Sensitivity Study Results.**

As expected, there is no dependency on mesh size in compression due to the lack of softening and there is dependency on mesh size in tension in order to ensure fracture energy is not overcounted. A similar pattern is exhibited in shear, but an anomalous case (Figure 2-12c) was discovered when the mesh size is 3 inches for the perpendicular to grain direction. It is not known what causes this discrepancy.

The second parametric study involved varying the rate of applied load with rate effects turned on. The default strain rate parameters for MAT_143 listed above are based on split Hopkinson pressure bar (SHPB) tests at strain rates of 500 and 1,000 $s^{-1}$. These strain rates are an order of magnitude greater than those anticipated in CLT exposed to blast loads. Thus, a series of single-element analyses were performed at strain rates associated with blast loading. Figure 2-13 documents the results of this strain rate study. It appears there is a sizable increase in strength for all force paths going from 0.5 to 5 $s^{-1}$. The magnitude of this increase appears to be excessive; further investigation on this point is warranted.

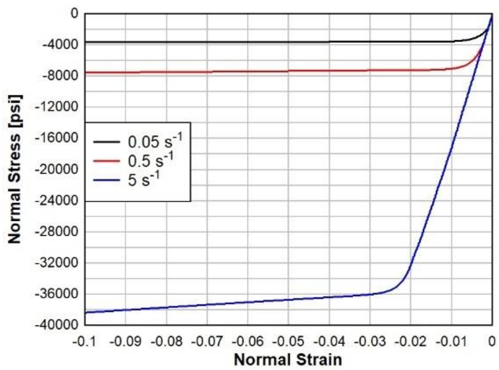


*(a) Compression Parallel to Grain.*

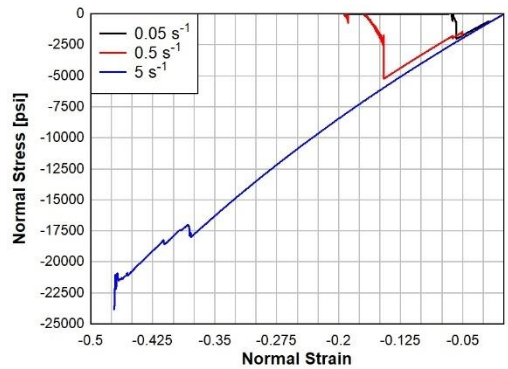


*(b) Compression Perpendicular to Grain.*

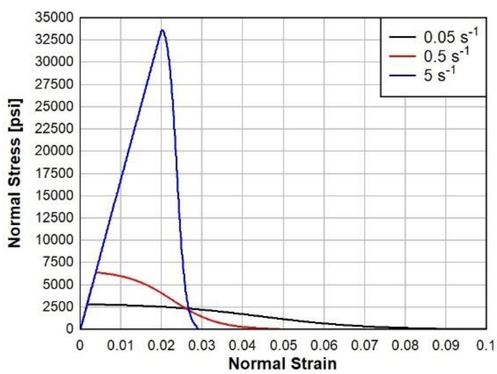


*(c) Tension Parallel to Grain.*

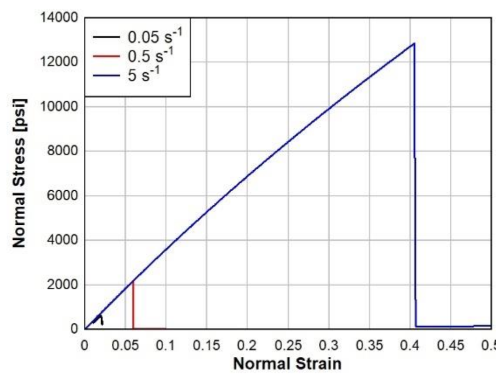


*(d) Tension Perpendicular to Grain.*

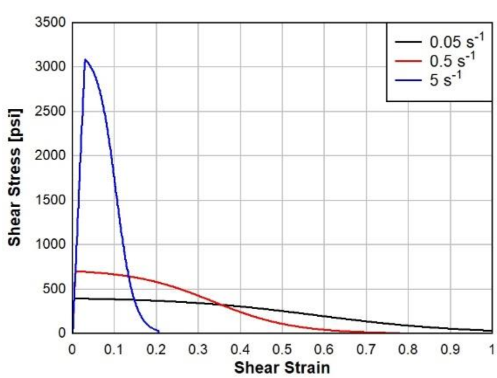


*(e) Shear Parallel to Grain.*

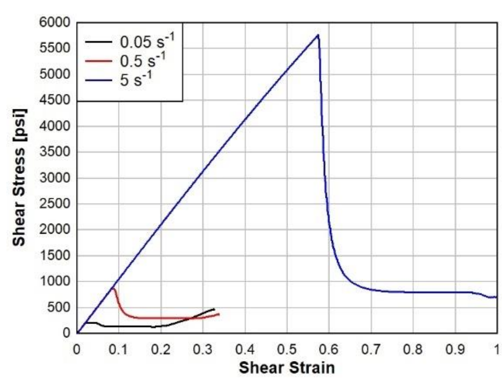


*(f) Shear Perpendicular to Grain.*

**Figure 2-13. Single-Element Strain Rate Study Results.**

# CHAPTER 3

# UMAINE QUASI-STATIC PANEL CALCULATIONS

This chapter describes a series of studies performed to evaluate the ability of HFPB models to compute results for quasi-static tests of CLT panels. These tests were performed at the University of Maine and are briefly described in Section 3.1. Section 3.2 details the construction of the finite element model by describing modeling decisions concerning ply-to-ply contact, finger joints, panel response following rupture, and other aspects of a CLT panel's unique characterization. Results from these models are presented in Section 3.3.

## 3.1 UNIVERSITY OF MAINE TESTING OVERVIEW

A testing program was performed at the University of Maine (UMaine) during Phase 1 that investigated the bending response of Grade V1 (3-ply and 5-ply), Grade E1, and Grade V4 CLT panels in their major strength direction under a uniformly-applied quasi-static load. The apparatus utilized for the testing was developed by UMaine and consisted of a series of rubber bladders filled with water capable of applying a uniform quasi-static pressure in a controlled fashion. This apparatus is shown with a CLT panel at the end of a test in Figure 3-1.

**Figure 3-1. UMaine Test Apparatus with CLT Panel at Conclusion of Test.**

The clear span of the CLT panel was 10 feet. CLT panels were allowed to rotate freely about their end supports for the tests modeled herein. Applied pressure, out-of-plane displacement, and total resisted load were measured and recorded as panels were displaced well beyond the displacement associated with peak panel strength. Tests were conducted in approximately 10 minutes with CLT panels having achieved roughly 10 inches of out-of-plane displacement. Plots of load (in terms of applied out-of-plane pressure) versus out-of-plane displacement for each CLT grade and ply configuration tested are shown in Figure 3-2.

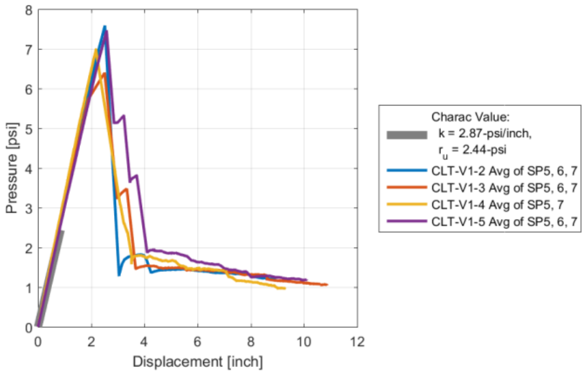


*(a) 3-Ply Grade V1.*

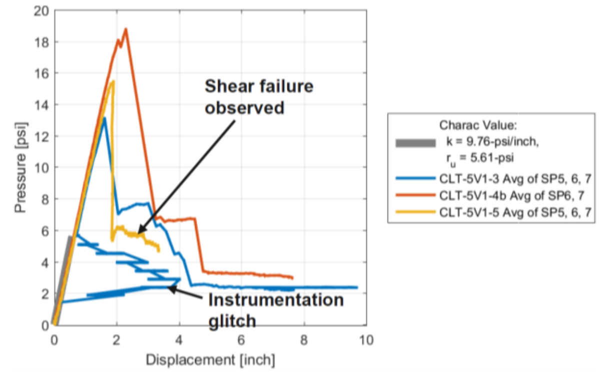


*(b) 5-Ply Grade V1.*

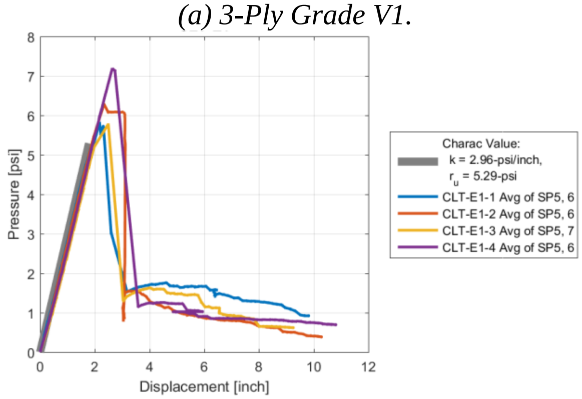


*(c) 3-Ply Grade E1.*

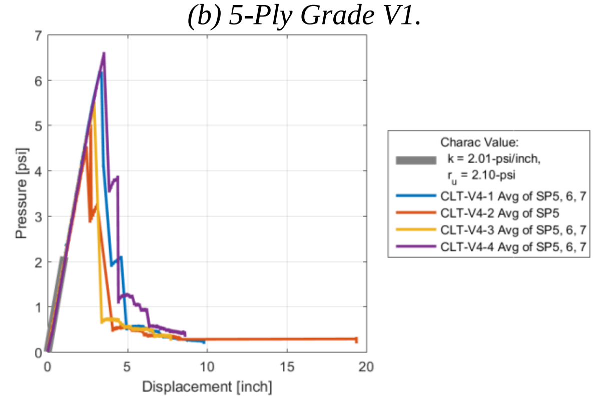


*(d) 3-Ply Grade V4.*

**Figure 3-2. UMaine Testing Load-Displacement Plot Results.**

*(SP = spring potentiometer gage)*

Typical failure pressures for 3-ply CLT panels were between 5 and 8 psi, corresponding to a total load of between 28,000 and 46,000 pounds of applied load. The 5-ply CLT panels failed with a pressure of around 15 psi or approximately 86,000 pounds of applied load. With one exception, all CLT panels failed near the panel's mid-span (a typical failure pattern is shown in Figure 3-1), presumably due to flexural stress. The location of panel rupture typically centered on knots, sloped grain, and finger joints (Figure 3-3). No shear slip between panel plies away from the location of panel rupture was observed. More information concerning the test setup, results, and conclusions from the UMaine testing is included in [1].

*(a) Sloped Grain.*

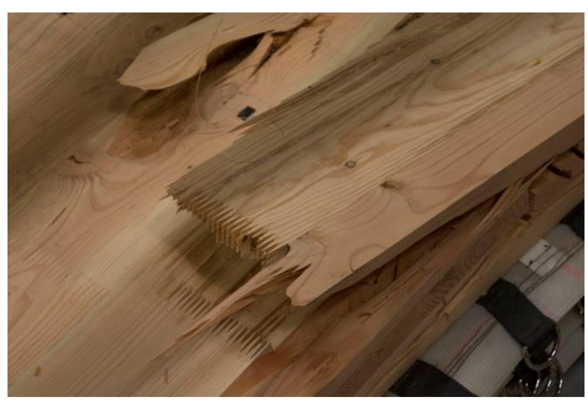

*(b) Finger Joint.*

**Figure 3-3. UMaine Testing Typical Panel Failure Locations.**

## 3.2 PANEL HFPB MODEL

The FE models of the 3-ply and 5-ply UMaine CLT panels described in the previous section are shown in Figure 3-4. The model was constructed using solid elements for the CLT panel, shell elements for the boundary supports, and solid elements for the water bag. Although the panel was 4 feet wide in the UMaine tests, only 21 inches of the panel was modeled to expedite computation time. Individual plies and finger joint locations were explicitly modeled in an attempt to capture the panel failure behavior observed in the UMaine tests. Elements were removed from the model (i.e., using the erosion feature in LS-DYNA) upon reaching a maximum effective principal strain of 0.6. More information concerning the CLT panel integration method type, ply modeling, finger joint modeling, boundary conditions, and loading protocol is provided in Sections 3.2.1 through 3.2.5.

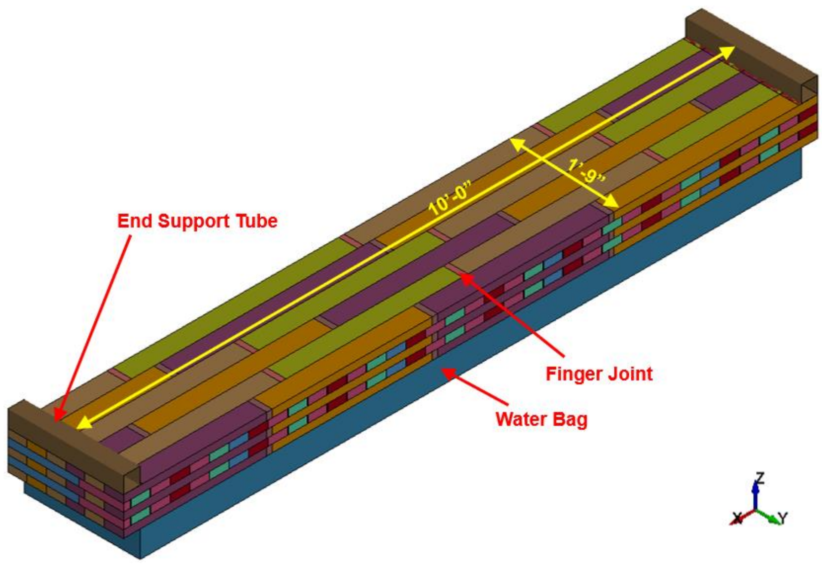


*(a) 3-ply.*

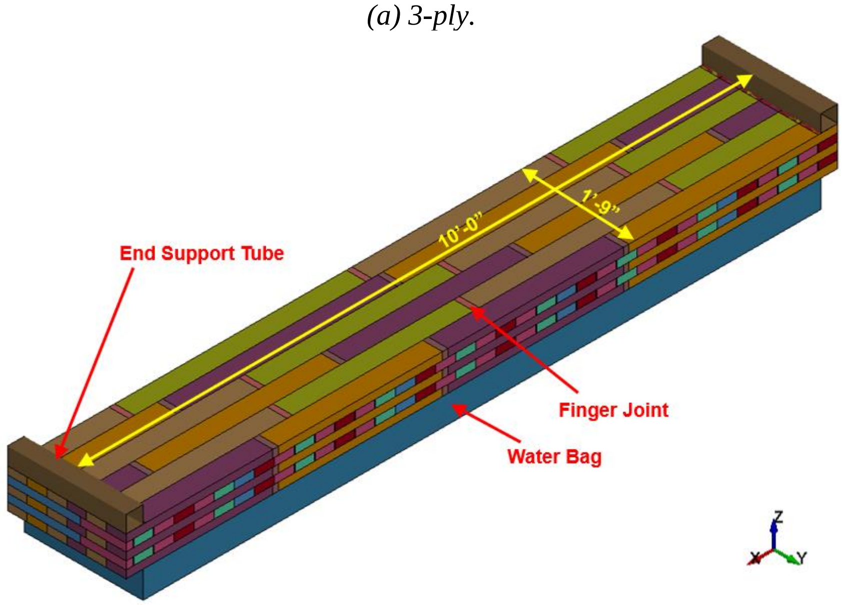


*(b) 5-ply.*

**Figure 3-4. UMaine Testing CLT Panel FE Models.**

### 3.2.1 Element Integration Type

Two types of integration were employed for the 8-node solid elements used to model the CLT panel: (1) single point and (2) selective reduced. Although single point integration is advantageous from a computational time perspective, when used with 8-node isoparametric solid elements some form of "hourglass" control is required to prevent zero-energy modes from destroying the computation. Hourglass control commonly involves incorporating artificial viscosity or stiffness into the isoparametric element, which is non-physical and thus introduces an inaccuracy into the computation that is difficult to assess. While selective reduced integrated solid elements by their nature do not require hourglass control, they are susceptible to shear locking (depending on the element aspect ratio) and are more expensive computationally. As such, it is a good idea to try different types of integration for the same problem to ascertain the extent that integration influences the results.

To evaluate the influence of the type of integration used in modeling the CLT panels, results were generated for models of the 3-ply Grade E1 panel. For the single point integration model, Flanagan-Belytschko stiffness hourglass control with exact volume integration was used; this is a commonly utilized hourglass control scheme and is described in Ref. [26]. Results in the form of out-of-plane applied pressure versus displacement for the two types of integration is shown in Figure 3-5. In general, the two integration types generate similar results in terms of initial stiffness, peak strength, and residual strength. Thus, either integration type could reasonably be used for this problem. The selective reduced integrated solid element was used for the remainder of the simulations described in this report since it avoided the introduction of non-physical modes of response without having to resort to hourglass control.

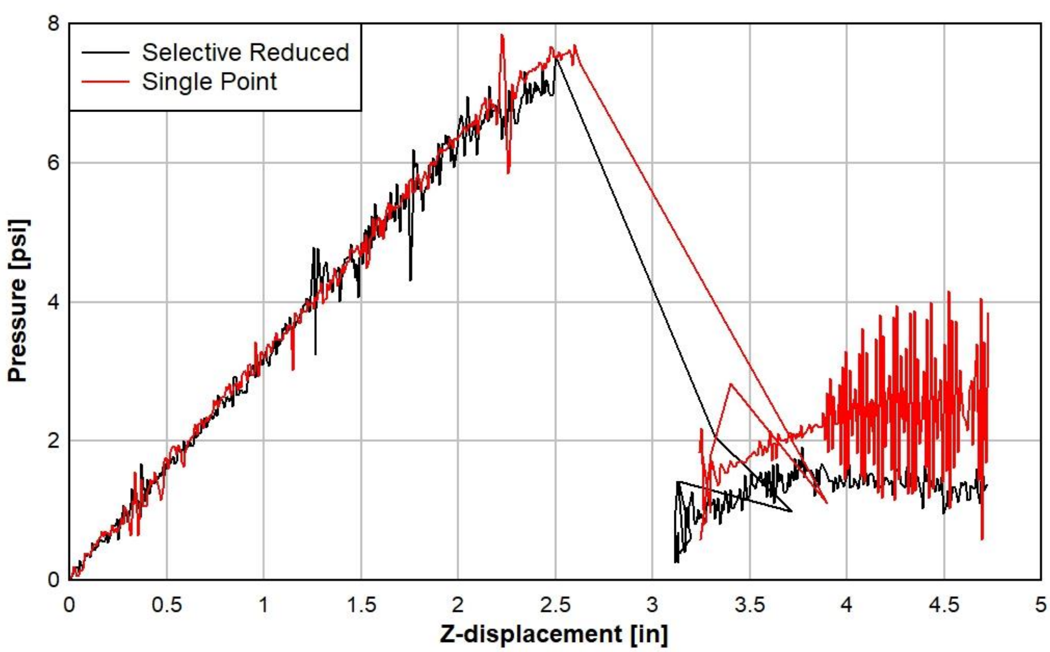


**Figure 3-5. Integration Type Study Results.**

### 3.2.2 Ply Modeling

During the UMaine tests, it was noticed that failure generally occurred in the CLT panel in individual boards at points of imperfection (e.g., finger joints, knots, sloped grain). Thus, instead of modeling a ply with a uniform sheet (i.e., like plywood), individual boards were modeled that were not tied and/or merged along their edges to adjacent boards. However, the connection between different plies was modeled using the tied contact option in LS-DYNA, which assumes that the shear stiffness of the adhesive is similar to or greater than that of the lumber and the shear strength of the adhesive exceeds that of the lumber. Results from the UMaine tests appeared to indicate both of these assumptions are reasonable.

A mesh size sensitivity study conducted with the 3-ply Grade V1 panel was performed to ensure that the element size selected would not deleteriously influence the results. Three mesh sizes were used:

- Mesh A: 1 inch by 1 inch in the flatwise direction; 3 elements through the thickness of the ply (i.e., 0.46-inch thick elements).
- Mesh B: 0.5 inch by 0.5 inch in the flatwise direction; 6 elements through the thickness of the ply (i.e., 0.23-inch thick elements).
- Mesh C: 0.5 inch by 0.5 inch in the flatwise direction; 4 elements through the thickness of the ply (i.e., 0.34-inch thick elements).

Figure 3-6 shows the three mesh sizes considered, while Figure 3-7 depicts the out-of-plane response for the three simulations in terms of applied pressure versus displacement. These results are quite similar. Thus, Mesh A was used for the remainder of the simulations described in this report.

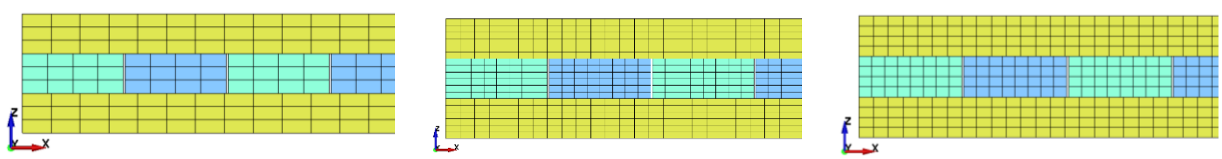

*(a) Mesh A.* *(b) Mesh B.* *(c) Mesh C.*

**Figure 3-6. Depiction of Mesh Sizes Used in Mesh Size Sensitivity Study.**

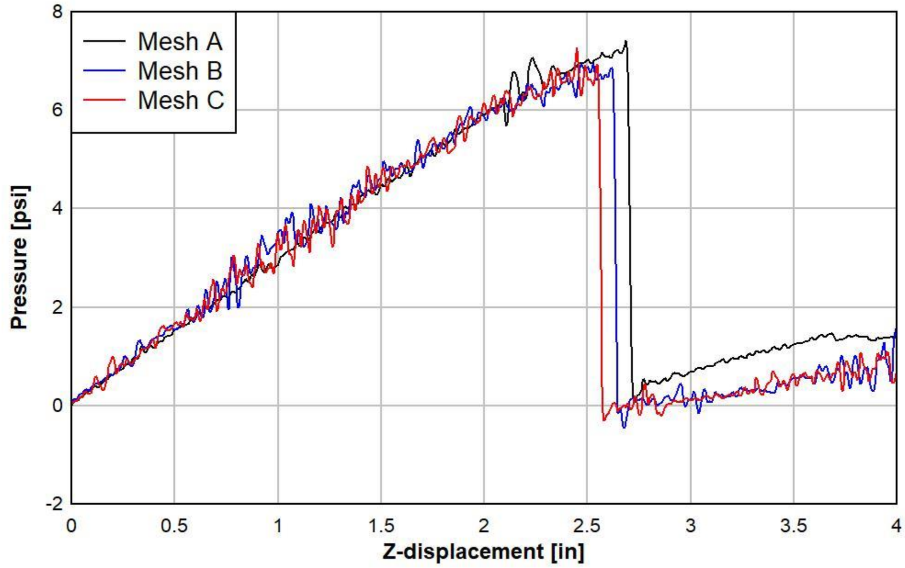


**Figure 3-7.  Mesh Size Sensitivity Study Results.**

### *3.2.3 Finger Joint Modeling*

Failures at the locations of the finger joints were observed repeatedly in the UMaine tests. Photos of failed finger joints for the Grade V1 and E1 panels are shown in Figure 3-8.  Thus, it was important to explicitly model the finger joints if the model would be expected to reproduce the observed failure.

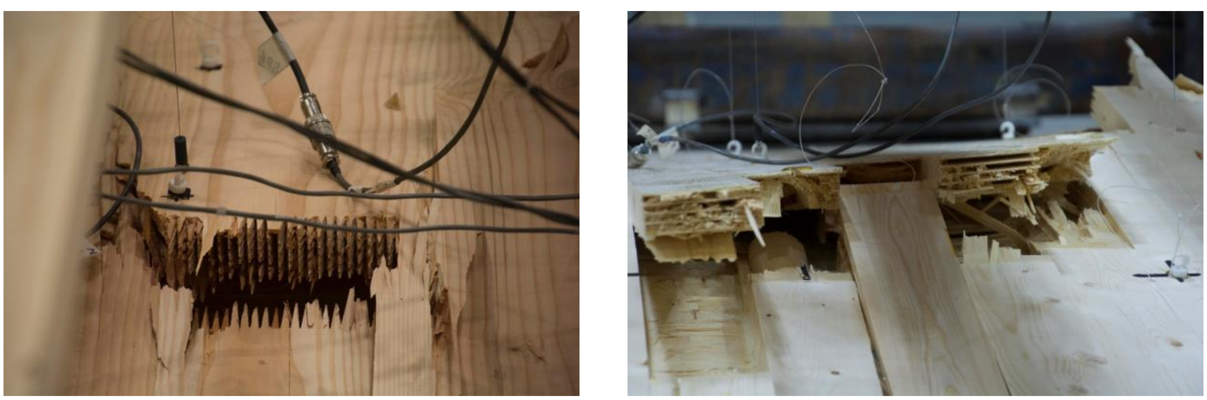

*(a) Grade V1.* *(b) Grade E1.*

**Figure 3-8.  UMaine Testing Finger Joint Failures.**

Finger joint testing has shown that scarf finger joints (i.e., those used in the UMaine panels) with slopes of 1 in 10 or 1 in 12 attain tensile strengths equal to 85 to 90 percent of the strength of clear wood [27].  Photographs of the UMaine panel figure joints indicate that the finger joint slope used in these panels was in this range.

Finger joints were randomly distributed throughout the panel model to roughly approximate the spacing and locations observed in the UMaine panels.  The finger joints were simply modeled with a line of elements that was made a different part.  The tension strength used for this line in the parallel to grain direction for the finger joint part was multiplied by 0.85. As there were no finger joints in the minor strength direction, this reduction factor was only utilized for finger joints in the major strength direction.

### 3.2.4 Boundary Conditions

The CLT panel is supported by an HSS3x3x1/8 at each end. The tube's support allowed the panel to freely rotate as intended in the UMaine testing. The HSS member is modeled with 0.5-inch square Hughes-Liu shell elements with an elastic steel material model. The nodes from the upper half of the tube were fixed in all six degrees of freedom (i.e., three translational and three rotational) to restrain this tube from moving, as shown in Figure 3-9.

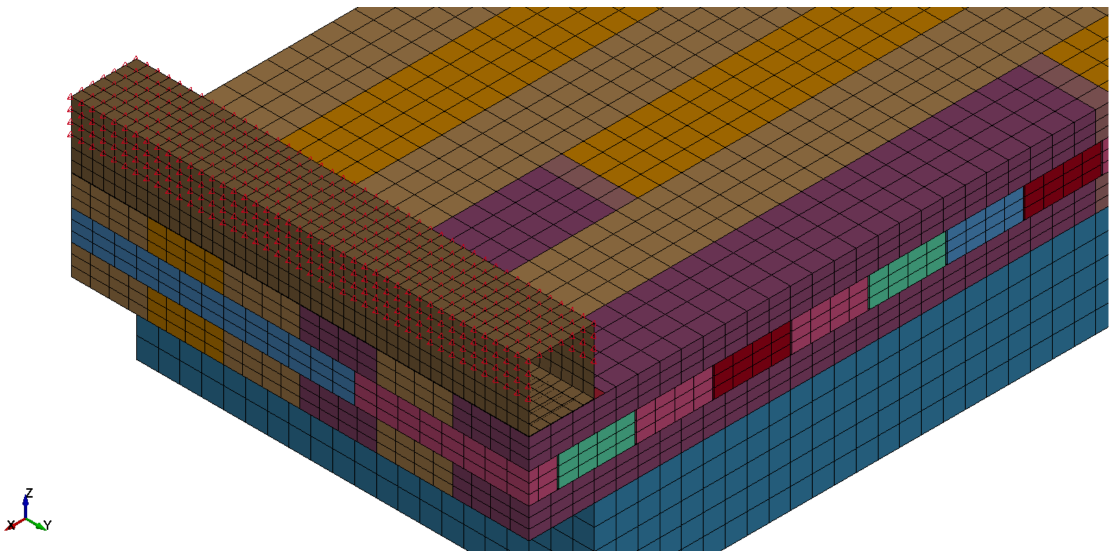


**Figure 3-9. UMaine Testing HFPB Model Boundary Condition.**

### 3.2.5 Loading Protocol

During the UMaine tests, CLT panels were pushed upward by a uniform pressure applied to the bottom face of the panel. The uniform pressure was applied by increasing the water pressure in a water bag at a set velocity over a 10-minute period. This water bag loading device was included in the analytic model, which allowed for the panel softening response and residual capacity to be explicitly modeled. The nodes on the boundary of the water bag were fixed in translation in the X and Y-directions. The nodes on the bottom of the water bag were moved upward (i.e., Z-direction) at a fixed velocity. The velocity was varied to assess the impact of the loading rate on the response of the Grade E1 CLT panel. Figure 3-10 shows the results of this loading rate study, which indicates that the loading rate does not significantly impact the response of the CLT panel. A loading rate of 0.25 inches per second was used for the remainder of the simulations described in this chapter.

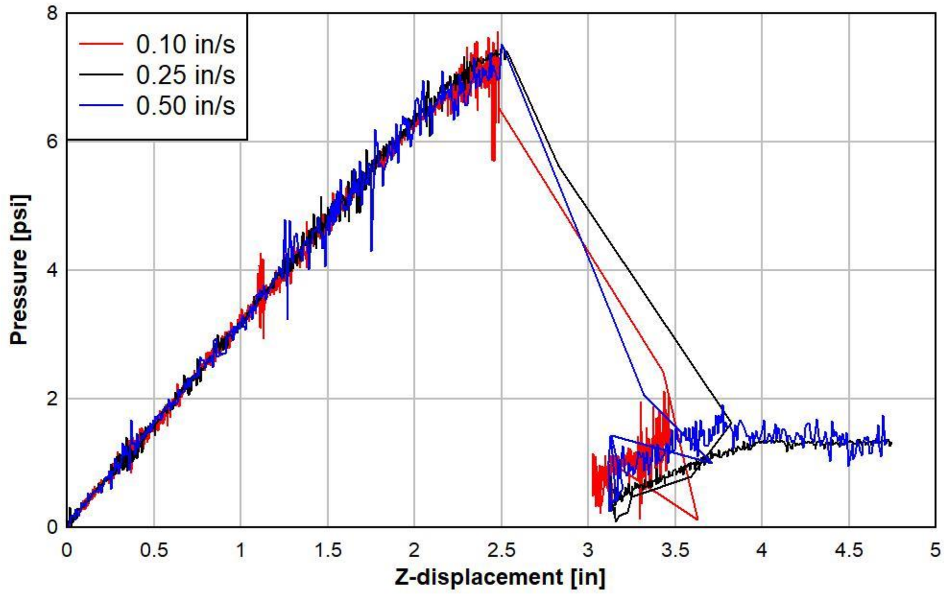


**Figure 3-10. Loading Rate Sensitivity Study Results.**

## 3.3 PANEL HFPB RESULTS

Figure 3-11 through Figure 3-14 compare the top surfaces of a panel after failure has occurred in the test and analytic model. These figures show representative test photographs and simulation screenshots for the 3-ply Grade E1, V1, and V4 and 5-ply Grade V1 CLT panels. It is noted that all four calculated results reproduce a semblance of the jagged top surface board failures observed in the tests.

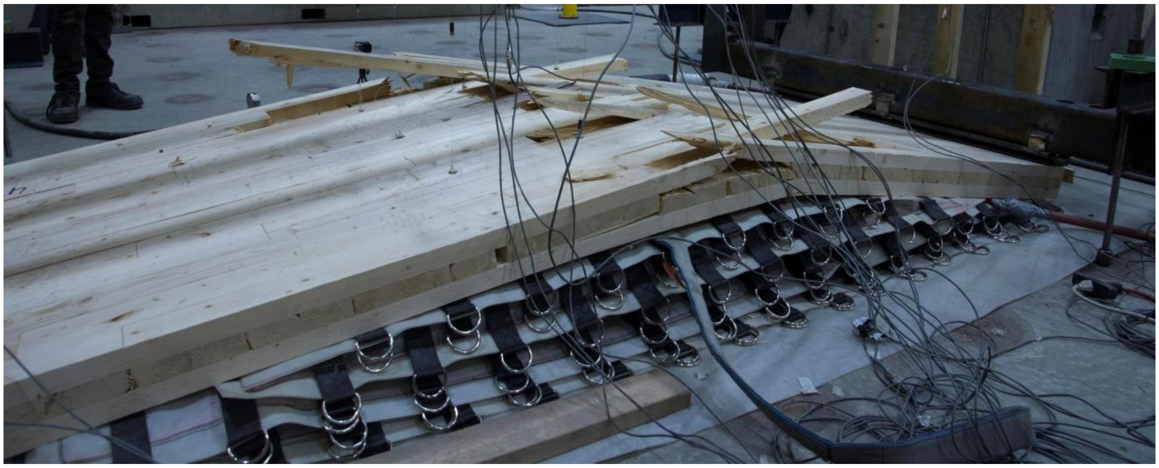

*(a) Post-test photograph (Test E1-3).*

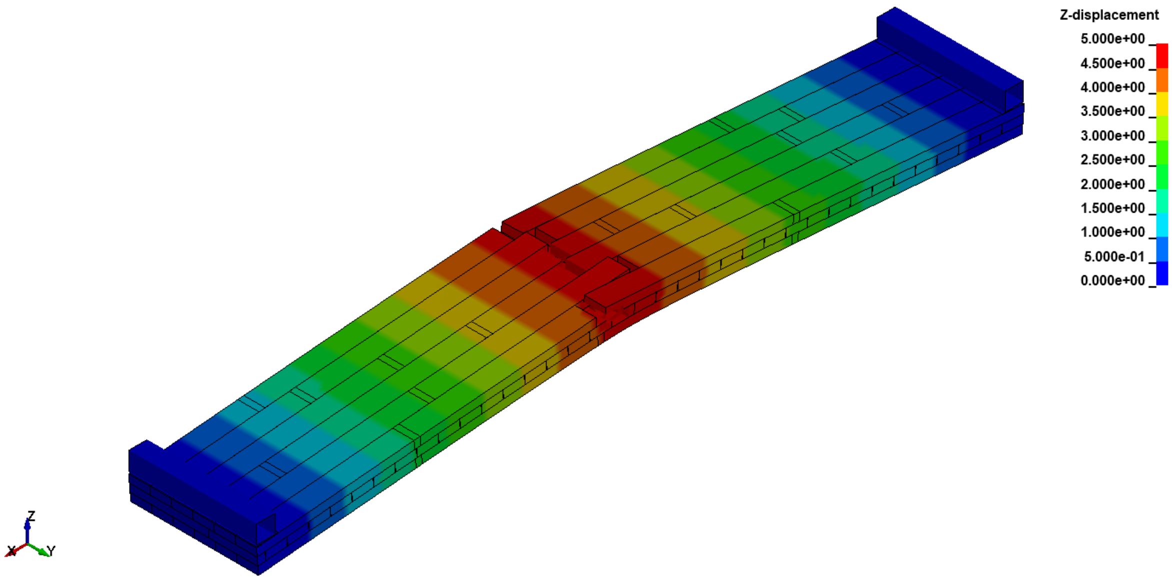


*(b) Simulation screenshot (resultant displacement in inches).*

**Figure 3-11. 3-Ply Grade E1 Panel Top Surface Comparison.**

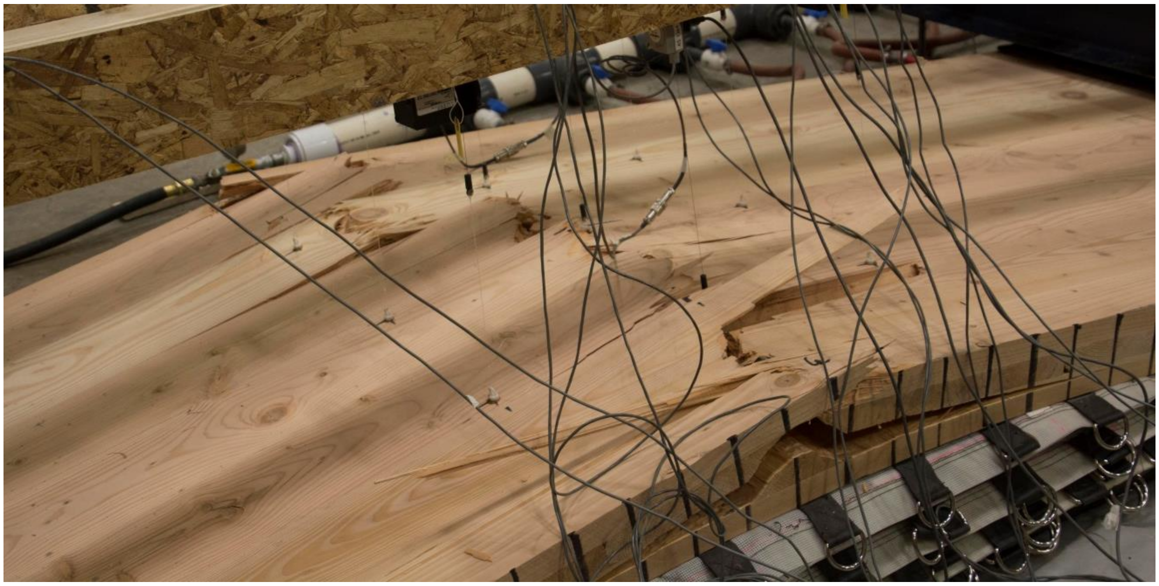

*(a) Post-test photograph (Test V1-3).*

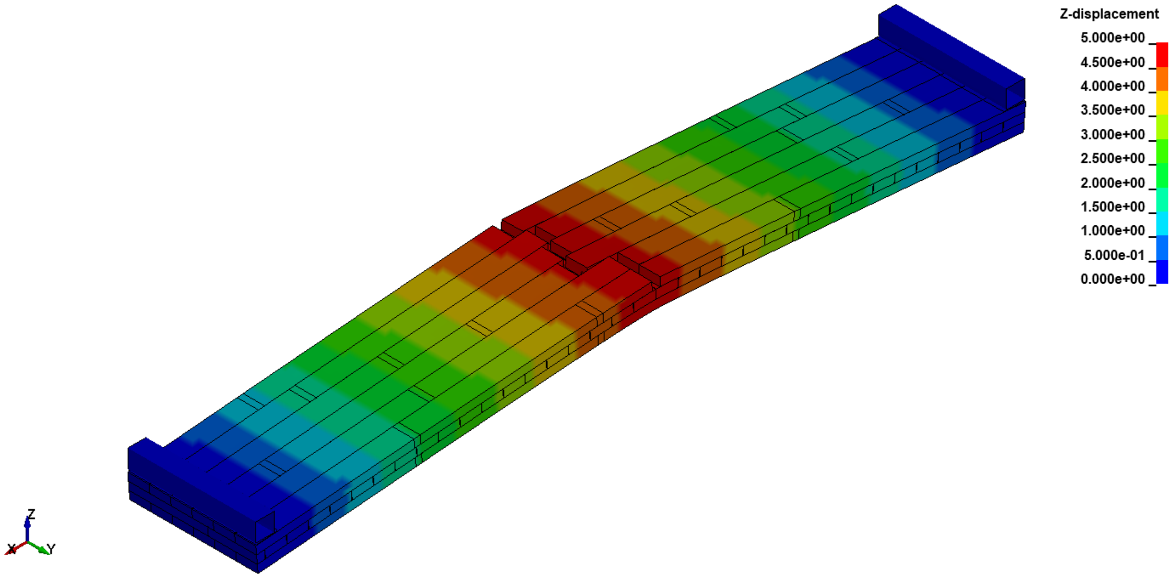


*(b) Simulation screenshot (resultant displacement in inches).*

**Figure 3-12. 3-Ply Grade V1 Panel Top Surface Comparison.**

*(a) Post-test photograph (Test V4-1).*

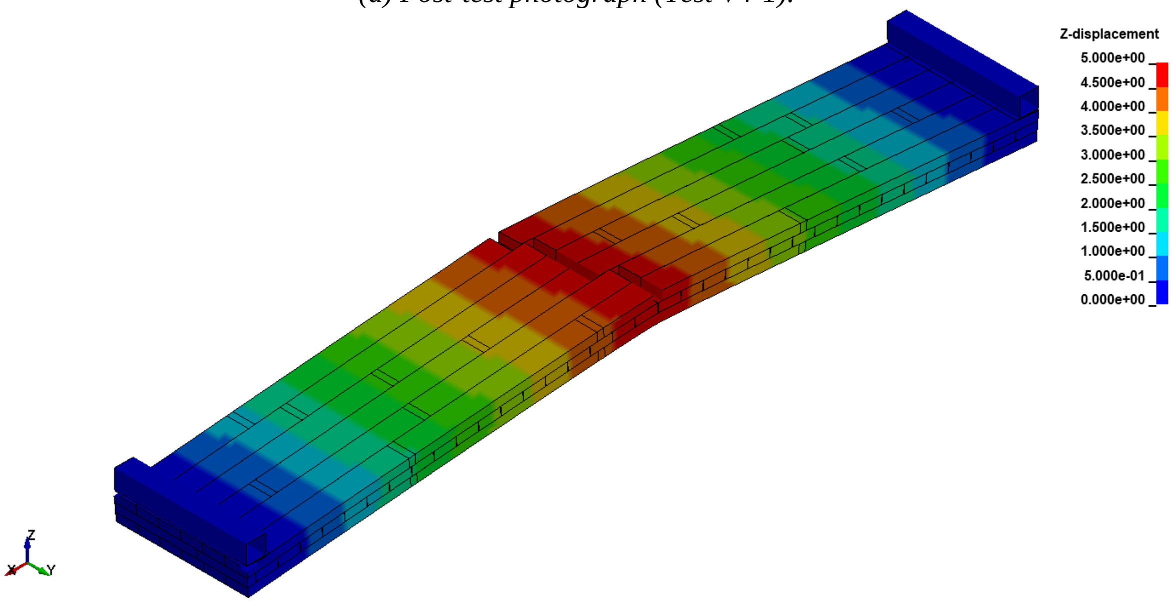


*(b) Simulation screenshot (resultant displacement in inches).*

**Figure 3-13. 3-Ply Grade V4 Panel Top Surface Comparison.**

*(a) Post-test photograph (Test 5V1-4).*

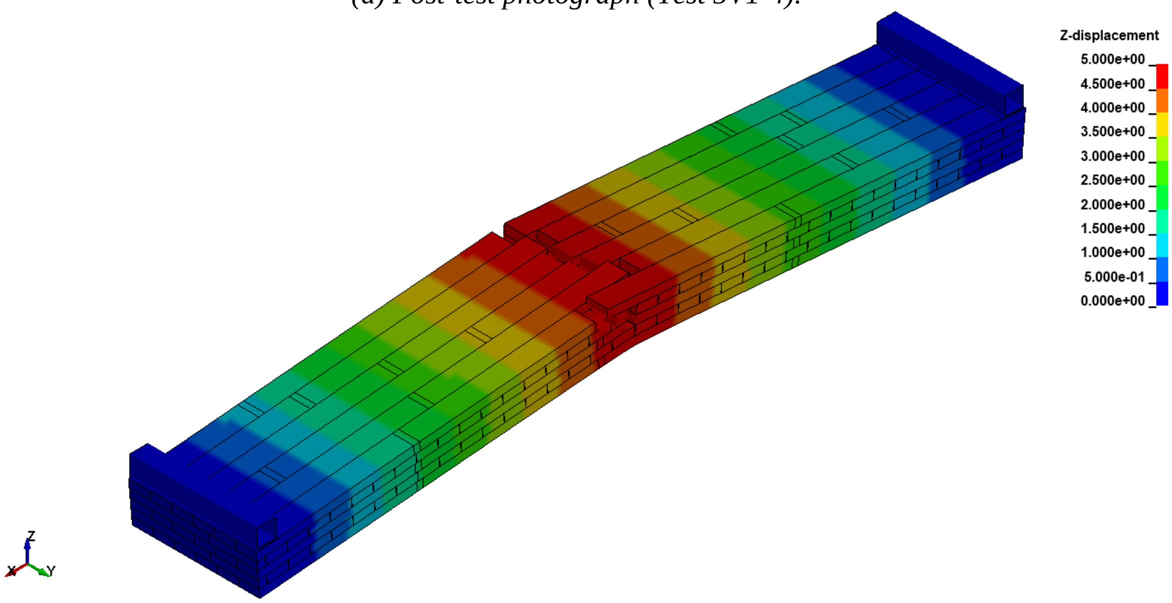


*(b) Simulation screenshot (resultant displacement in inches).*

**Figure 3-14. 5-Ply Grade V1 Panel Top Surface Comparison.**

The out-of-plane pressure versus displacement responses computed by the HFPB models of the panels are depicted in Figure 3-15. The test data obtained from the University of Maine along with its average is plotted alongside the analytic results for comparison purposes. The following observations may be made:

- The computed elastic panel stiffness is either slightly larger (e.g., 3-ply Grade E1) or very similar (e.g., 3-ply Grade V1) to those measured in the tests.

- The computed peak panel strength is roughly 20 percent larger than the average test value for the 3-ply Grade E1 panel, very similar to the average test values for the Grade V1 panels, and roughly 20 percent smaller than the average test value for the 3-ply Grade V4 panels.

- The HFPB calculations well approximate the average residual capacity test values of the CLT panels irrespective of grade and ply number. Additionally, the 5-ply panel computation exhibits the stepped post-peak response observed in the tests.

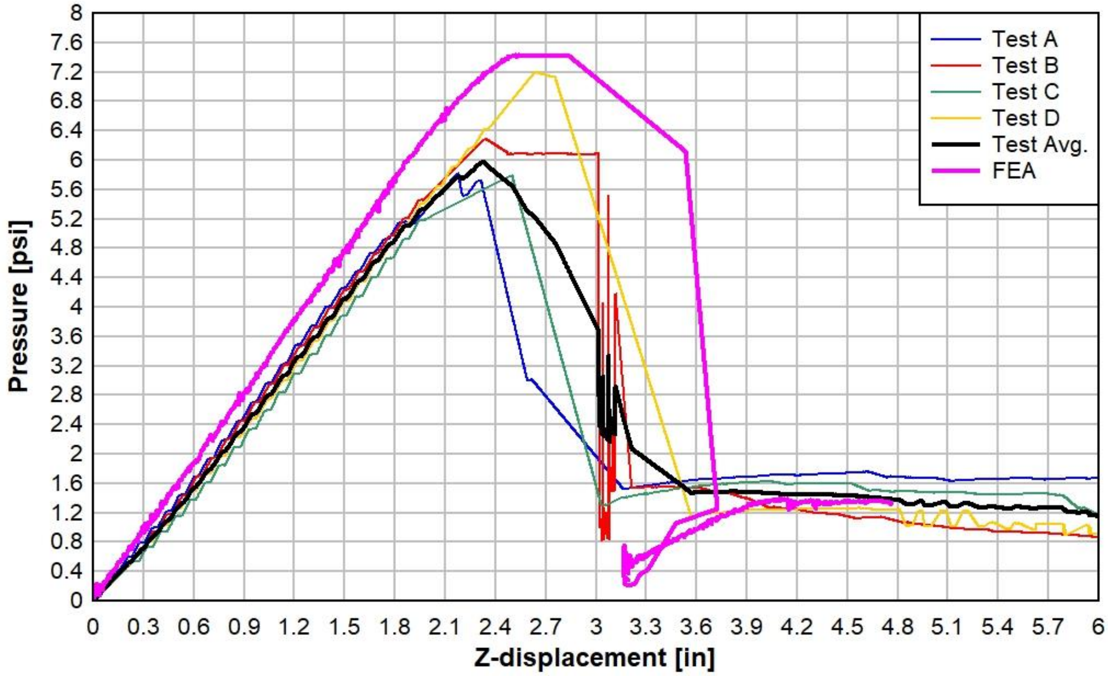


*(a) Grade E1, 3-ply.*

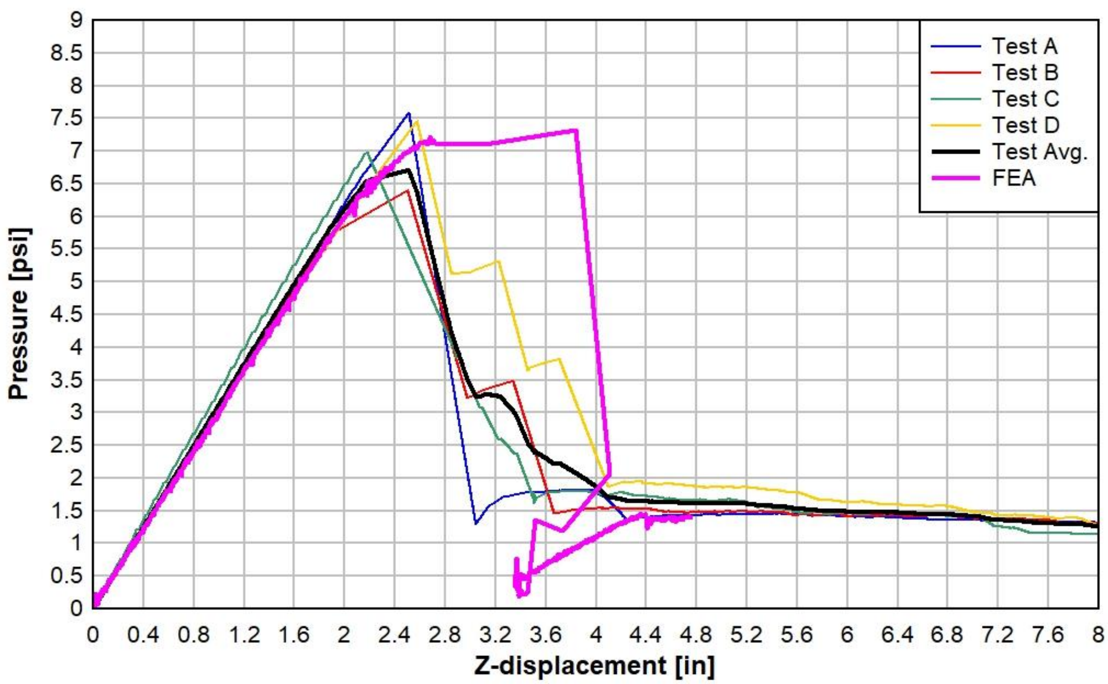


*(b) Grade V1, 3-ply.*

**Figure 3-15. UMaine Testing Load vs. Displacement Comparison Plots.**

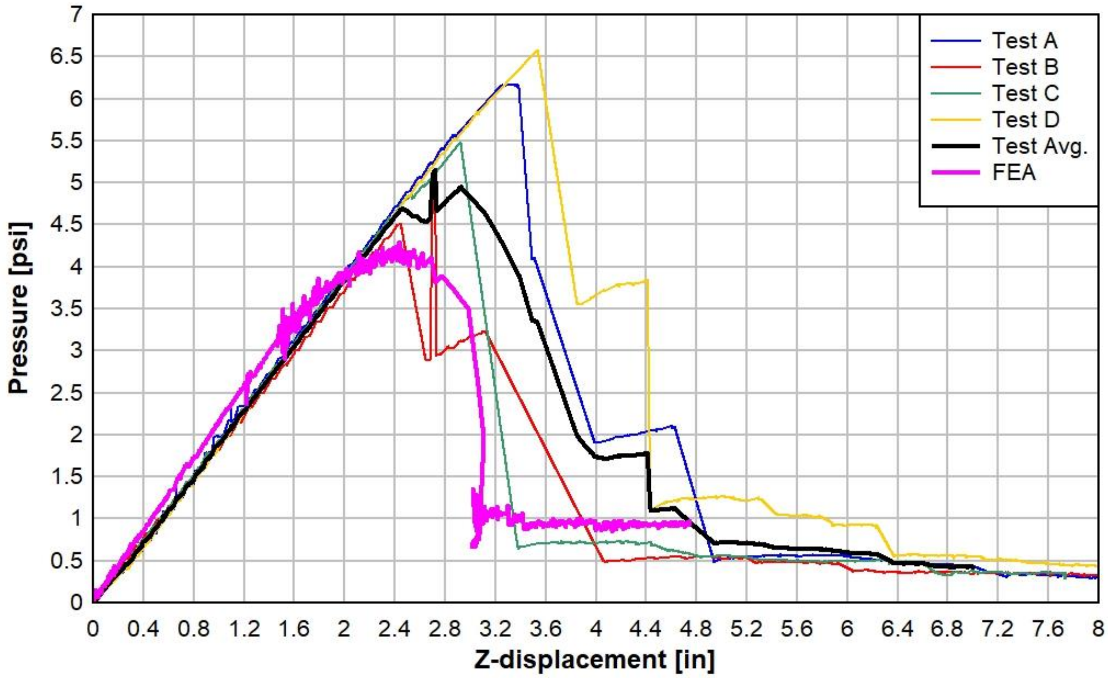


*(c) Grade V4, 3-ply.*

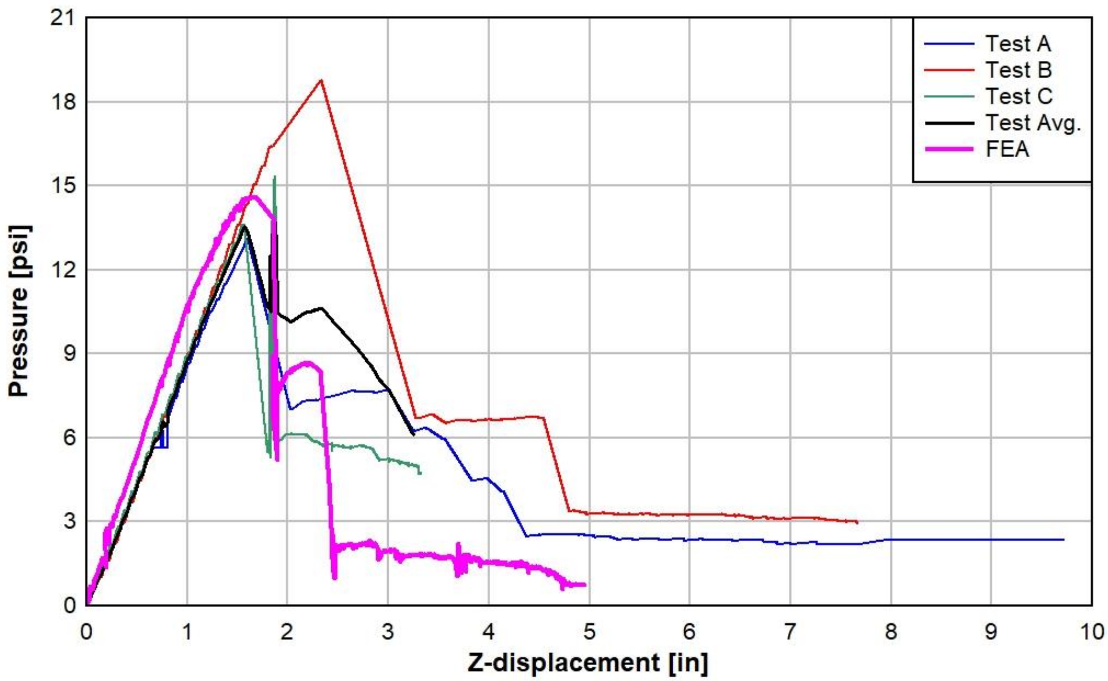


*(d) Grade V1, 5-ply.*

**Figure 3-15. UMaine Testing Load vs. Displacement Comparison Plots. (Cont'd)**

# CHAPTER 4

# AFCEC QUASI-STATIC PANEL CALCULATIONS

This chapter describes a series of analyses performed to evaluate the capability of HFPB models to compute results for the quasi-static tests conducted at AFCEC using their load tree testing apparatus. The primary purpose of these calculations was to assess the ability of MAT_143 to reproduce panel responses under bi-axial stress states. The material model and its fit were described in Chapter 2 and the development of the CLT panel model (i.e., element integration type, mesh size, ply connectivity, and finger joints) was described in Chapter 3.

The AFCEC tests are briefly described in Section 4.1. The construction of the FE model and decisions concerning boundary conditions are described in Section 4.2. The results obtained from these simulations are shown in Section 4.3.

## 4.1 AFCEC TESTING OVERVIEW

A testing program was performed at AFCEC during Phase 2 that investigated the flatwise bending response of axially-loaded CLT panels in the major strength direction under a uniformly-applied transverse quasi-static load. Tests were performed on CLT panels of different grades (i.e., E1, V1, and V4), ply numbers (i.e., 3-ply and 5-ply), axial loads, and panel lengths (i.e., 12 feet and 14 feet).

The tests that were modeled were 12-foot long, 3-ply Grade V1 panels with axial loads varying from 0 to 40 percent $F_c^*$, where $F_c^*$ is the ASD reference axial compressive stress, $F_c$, noted in manufacturer's literature (i.e., Ref. [20]) multiplied by all applicable NDS adjustment factors except the column stability factor, $C_P$. (For the 0% $F_c^*$ case, although no axial load was applied to the CLT panel by the horizontally-oriented actuator, the load platens were fixed translationally and thus passively imparted axial load as the panel was displaced upward.)

The load tree testing apparatus at AFCEC is shown with a CLT panel at the end of a test in Figure 4-1. This apparatus uses actuator-controlled cylindrical steel tubes to apply a progressively-increasing uniform out-of-plane load by pulling test panels upwards while simultaneously applying a constant axial load via another actuator.

The ends of the CLT panels were supported by an L6x4x3/4 angle with its long leg oriented vertically. As such, the unsupported span for the 12-foot long test panels was 136 inches. This angle and its connection were designed to remain elastic for all tests performed.

Tests were initiated by loading the panels in the in-plane (axial) direction up to the prescribed axial load at a maximum rate of 1,000 pounds per minute. Once the axial load was reached, the panels were then displaced upward at a rate of 0.5-inch/min using the collection of steel tubes shown in Figure 4-1. Axial load was maintained in the panel via force control except for panels with no predefined axial load (i.e., 0% $F_c^*$ case). Tests were typically completed within 15 minutes.

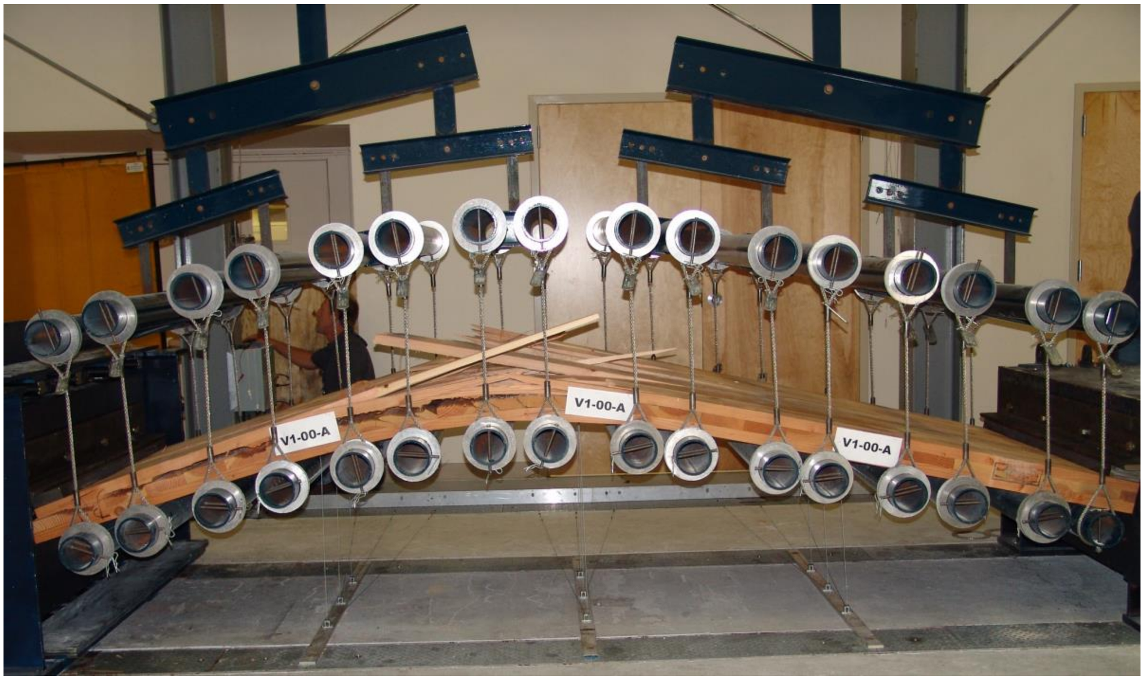


**Figure 4-1. AFCEC Test Apparatus with CLT Panel at Conclusion of Test.**

Results in terms of applied out-of-plane pressure versus out-of-plane displacement are shown in Figure 4-2 for the 12-foot long, 3-ply Grade V1 CLT panels for six levels of axial load. Several comments concerning these results include:

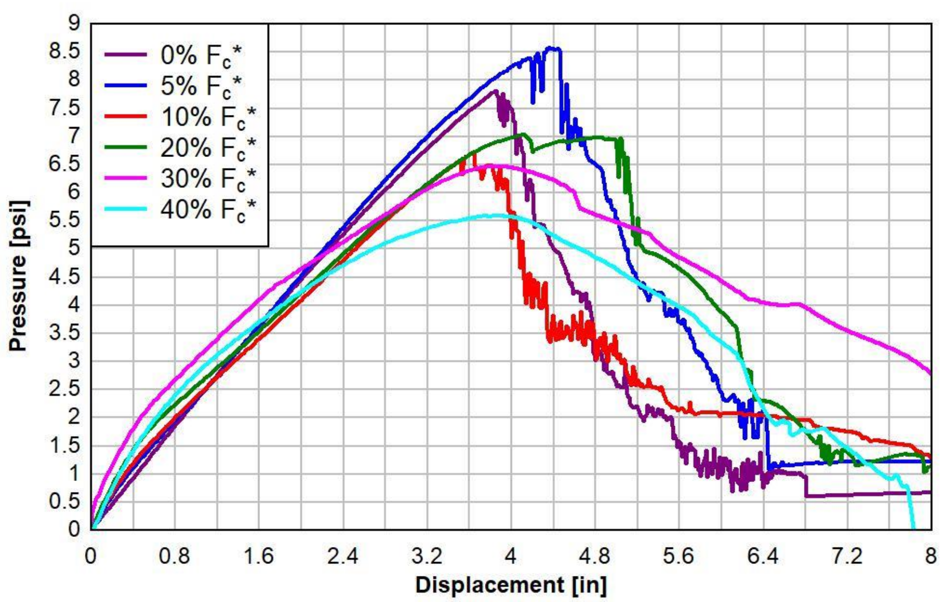


**Figure 4-2. Load-Displacement Plot Results for 12-ft Long, 3-Ply Grade V1 CLT Panels with Axial Load.**

- It is apparent that increasing the axial load generally results in a reduced flatwise bending strength. However, a small amount of axial load appears to enhance the strength of the panel over that associated with pin-roller boundary conditions.

- That a small amount of axial load is potentially helpful could be tied to several structural phenomena: (1) compression membrane action (i.e., for the 0% $F_c^*$ case), (2) panel arching due to axial load (i.e., for the 5% $F_c^*$ case), (3) decrease of tension bending stress due to a pre-compression load, and (4) rotational restraint due to means used to apply the axial load.

- The loading stiffness for the 0% $F_c^*$ and 5% $F_c^*$ cases is noticeably higher than that for the remaining cases. Not surprisingly, these are the cases in which negligible localized damage was observed at the ends of the panels (Figure 4-3a) when compared to other tests (Figure 4-3b).

- The greater the axial load, the earlier the stiffness begins to decrease prior to reaching peak strength. This result implies that the bottom of the panel is "failing" in compression (e.g., crushing). Although no visible signs of crushing were observed following the tests, it is interesting to compare the damage patterns at the top of the panel at mid-span across several axial loads. Figure 4-4a and Figure 4-4b provides photographs for top of panel damage for 10% $F_c^*$ and 40% $F_c^*$, respectively. Comparing the photographs indicates that the damage associated with 40% $F_c^*$ is localized around a central "hinge" at panel mid-span while the 10% $F_c^*$ failure is concentrated at finger joints and other material imperfections.

- Furthermore, comparing the softening stiffnesses following peak response with axial load indicates there is more ductility associated with the higher axial load failures, further supporting the supposition that a relatively ductile compression crushing response is controlling over a more brittle tension rupture response.

More information concerning the test setup, results, and conclusions from the AFCEC load tree testing is included in [3].


*(a) 5% $F_c^*$ – no evidence of panel edge failure.*

*(b) 10% $F_c^*$ – failure at top fibers due to rotational constraint provided by test apparatus.*

**Figure 4-3. Damage at Ends of CLT Panel for Various Axial Loads.**

(a) 10% $F_c^*$. (b) 40% $F_c^*$.

**Figure 4-4. Damage at Mid-Span of CLT Panel for Various Axial Loads.**

## 4.2 PANEL HFPB MODEL

The HFPB model of the 3-ply CLT panels described in the previous section is shown in Figure 4-5. The model is identical to that used for the UMaine testing simulations except the panel length was increased to 12 feet. Decisions concerning element integration type, mesh size, and loading rate were kept the same as those used in the UMaine panel model. The only modeling feature that markedly changed from the UMaine panel simulations was the boundary conditions, where an the axial load was applied to the CLT panel and some level of end restraint transpired.

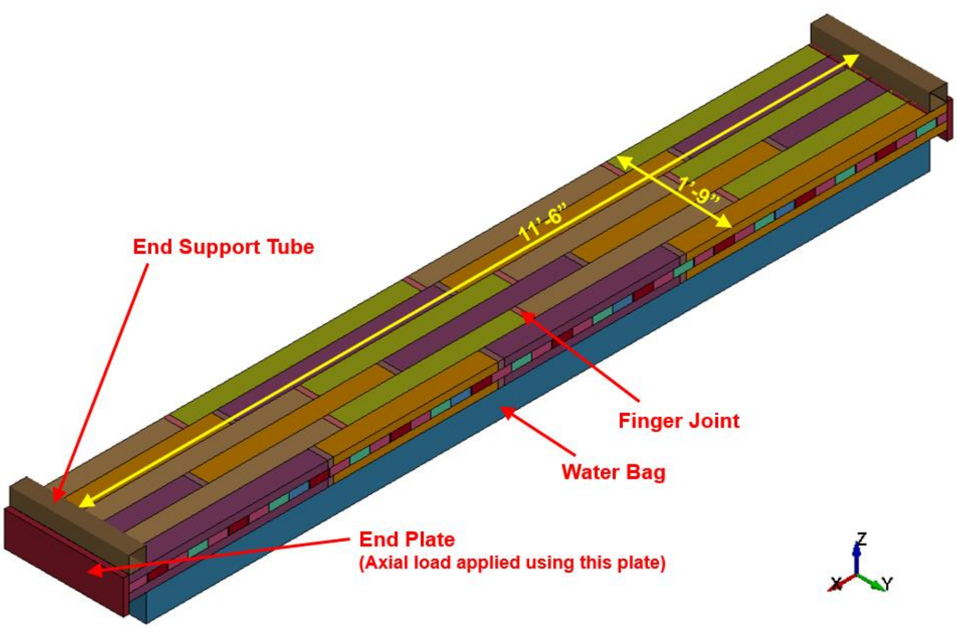


**Figure 4-5. AFCEC Testing CLT Panel HFPB Model.**

### 4.2.1 Boundary Conditions

Transverse support was provided by an HSS3x3x1/8 tube as for the UMaine panel model. (It should be noted that while the calculation used a 3-inch long support leg, the test used a 4-inch long support leg. This deviation causes the clear span to be slightly off between the calculation and the test – 138 inches versus 136 inches, respectively.)

An end plate was employed through which the axial load was applied. For all calculations except for the 0% $F_c^*$ case, axial load was applied using a force boundary condition on the far side of the end plate. For the 0% $F_c^*$ case, the nodes on the far side of the end plate were simply fixed in the three translational degree of freedom directions. Figure 4-6 compares the measured axial loads from the tests (dashed lines) with the computed axial loads in the panel (solid lines). (The computed axial loads are measured on the panel side of the end support tube). Two observations are of note:

- For all calculations except for the 0% $F_c^*$ case, the axial force in the panel is not constant in contrast with the applied boundary condition force. This slight deviation is expected considering that the normal force between the panel and end support tube is not constant and will serve to catch axial force due to friction.

- For the 0% $F_c^*$ case, a significant discrepancy is observed between the computed and measured (test) axial force values. This deviation is likely due to variational "slop" in the test setup that would serve to reduce the measured axial load in the test.

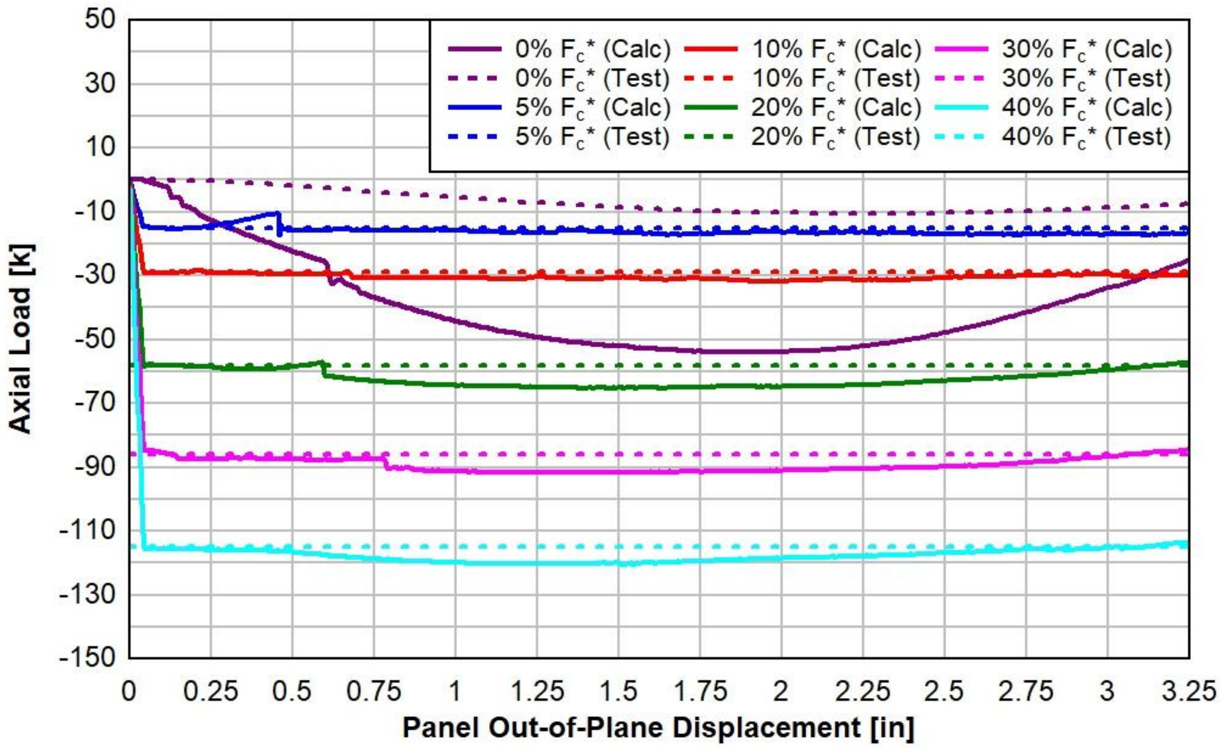


**Figure 4-6. AFCE Testing Applied vs. Computed Panel Axial Forces.**

## 4.3 PANEL HFPB RESULTS

Figure 4-7 through Figure 4-12 compare the top surfaces of failed panels via representative test photographs and simulation screenshots for axial loads of 0% $F_c^*$, 5% $F_c^*$, 10% $F_c^*$, 20% $F_c^*$, 30% $F_c^*$, and 40% $F_c^*$, respectively.

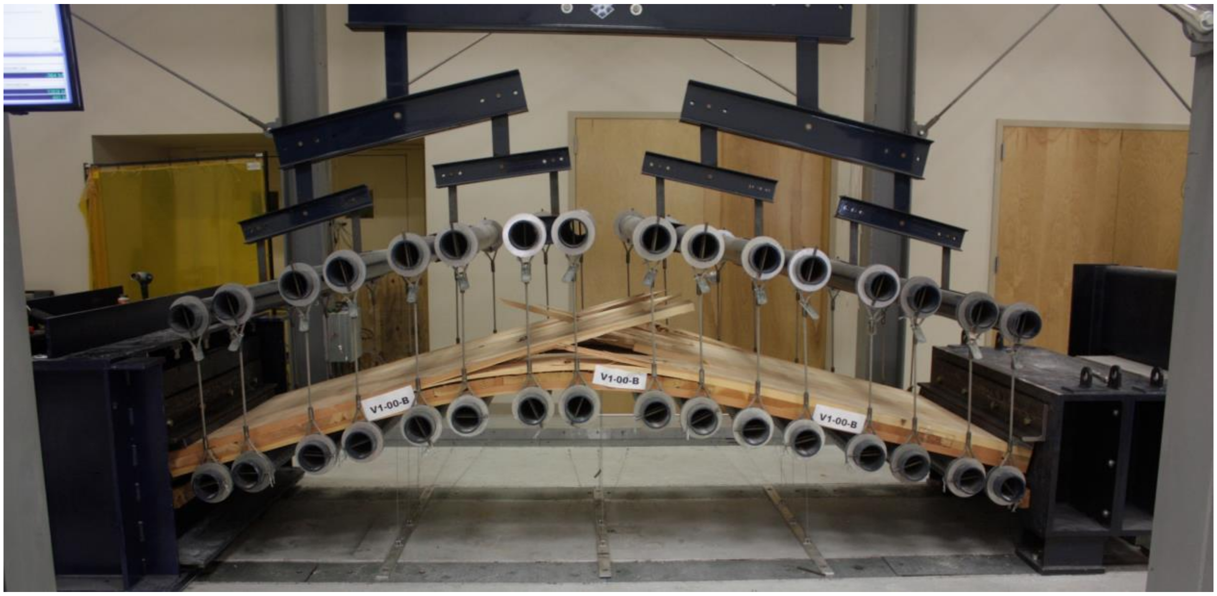


*(a) Post-test photograph (Test V1-00-B).*

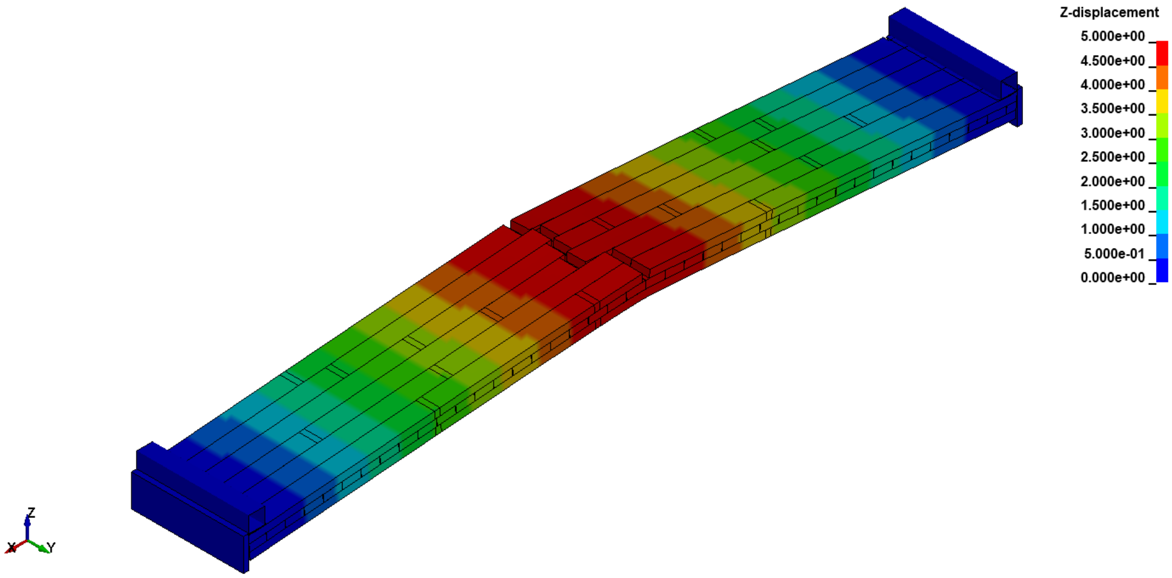


*(b) Simulation screenshot (resultant displacement in inches).*

**Figure 4-7. 3-Ply Grade V1 Panel Top Surface Comparison (0% $F_c^*$).**


*(a) Post-test photograph (Test V1-05-A).*

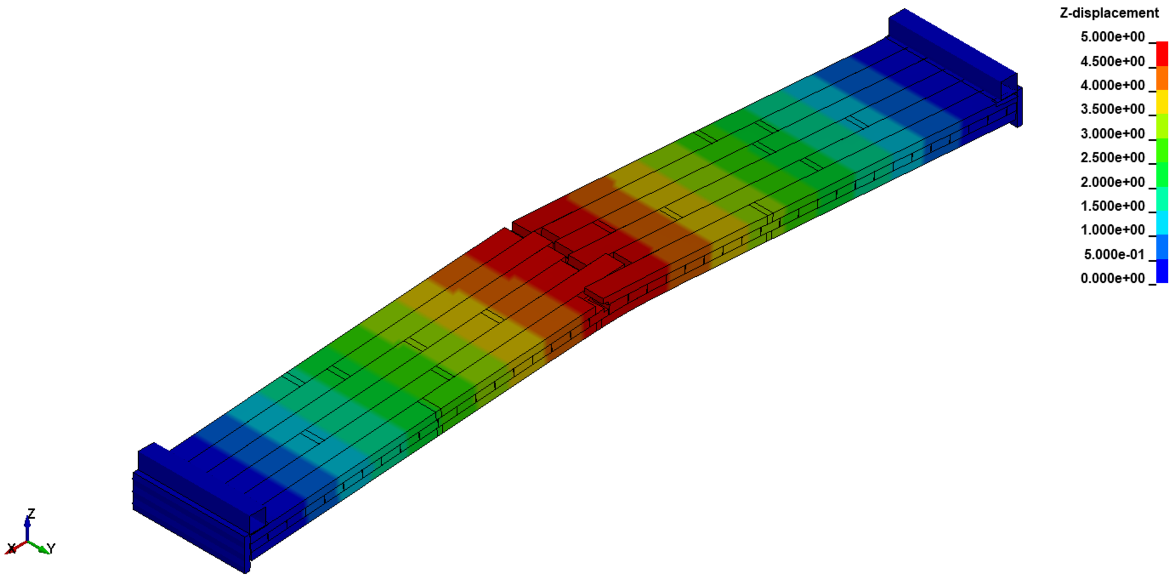


*(b) Simulation screenshot (resultant displacement in inches).*

**Figure 4-8. 3-Ply Grade V1 Panel Top Surface Comparison (5% $F_c^*$).**

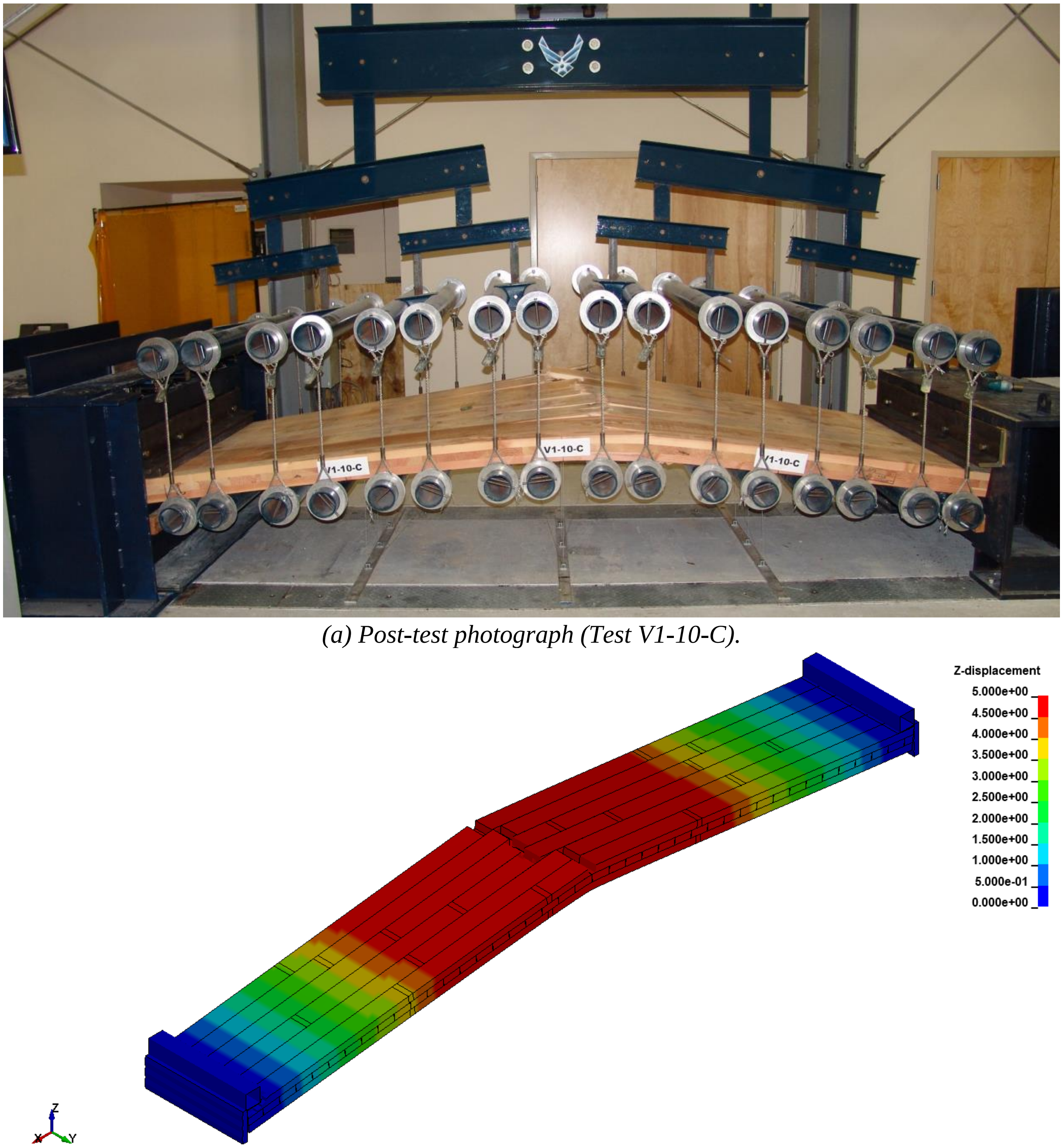


*(a) Post-test photograph (Test V1-10-C).*

*(b) Simulation screenshot (resultant displacement in inches).*

**Figure 4-9. 3-Ply Grade V1 Panel Top Surface Comparison (10% $F_c^*$).**

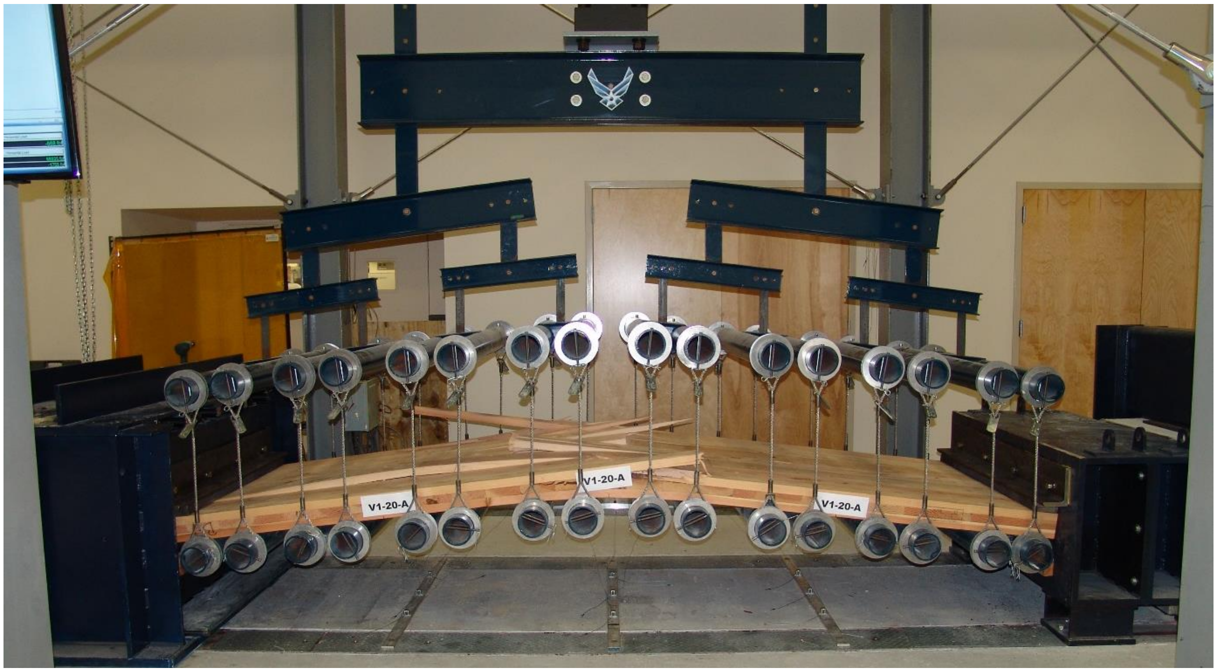


*(a) Post-test photograph (Test V1-20-A).*

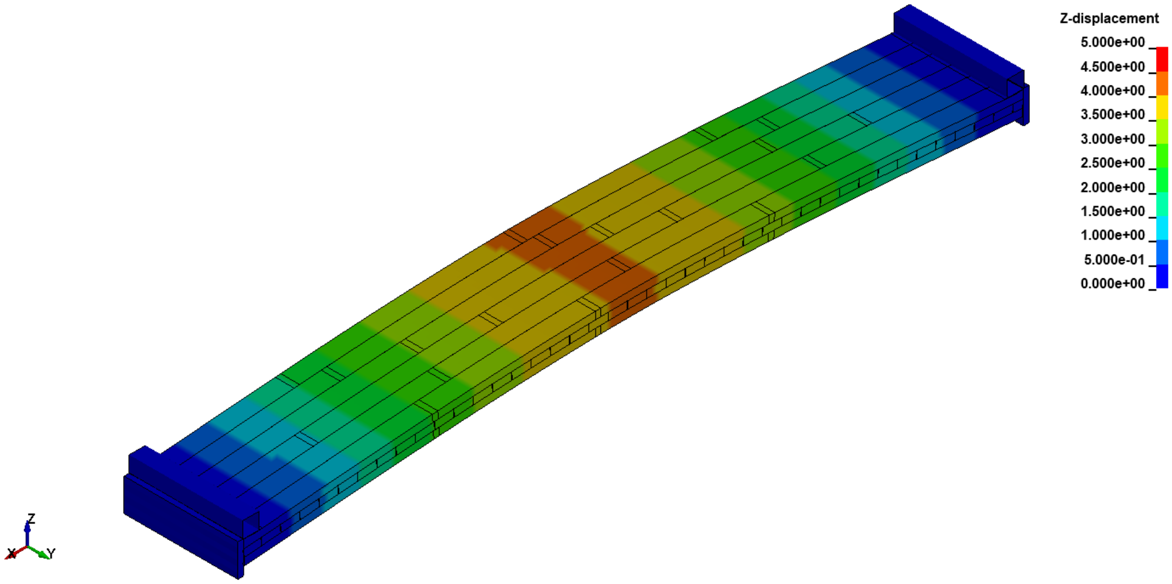


*(b) Simulation screenshot (resultant displacement in inches).*

**Figure 4-10. 3-Ply Grade V1 Panel Top Surface Comparison (20% $F_c^*$).**


*(a) Post-test photograph (Test V1-30-A).*

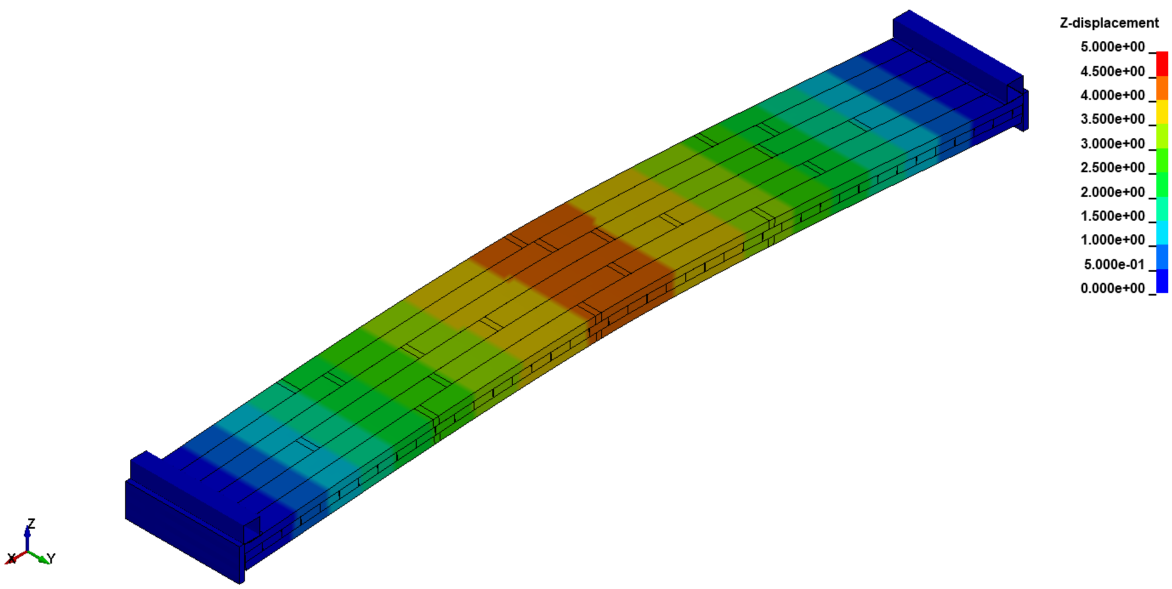


*(b) Simulation screenshot (resultant displacement in inches).*

**Figure 4-11. 3-Ply Grade V1 Panel Top Surface Comparison (30% $F_c^*$).**

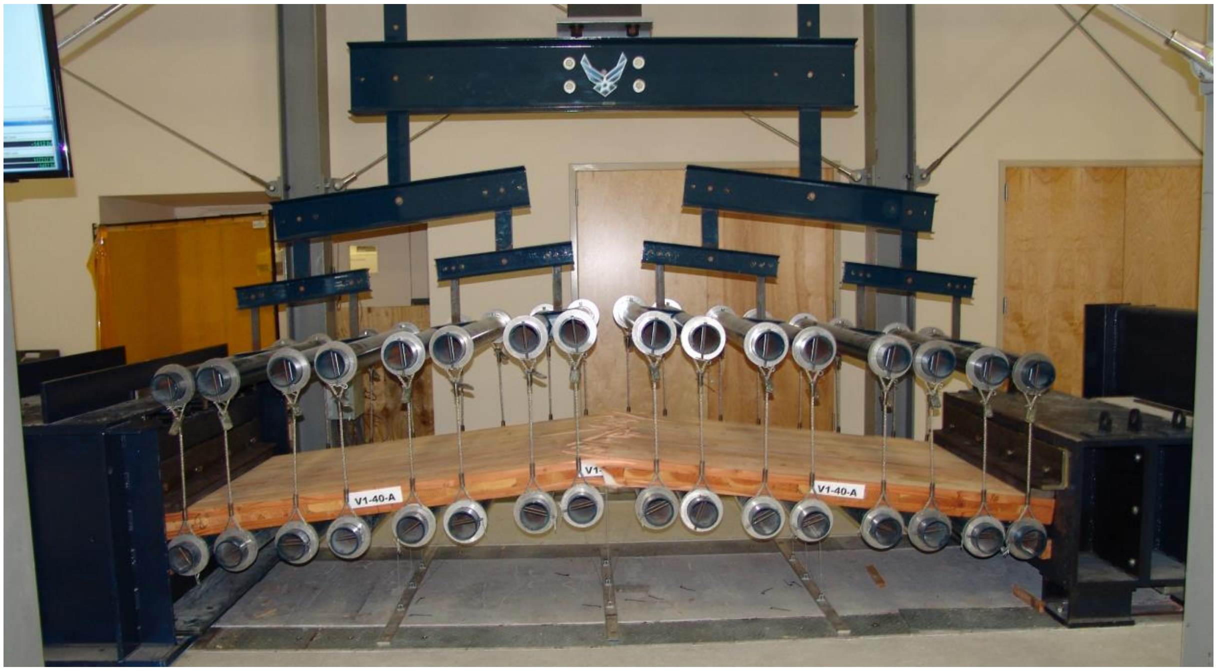


*(a) Post-test photograph (Test V1-40-A).*

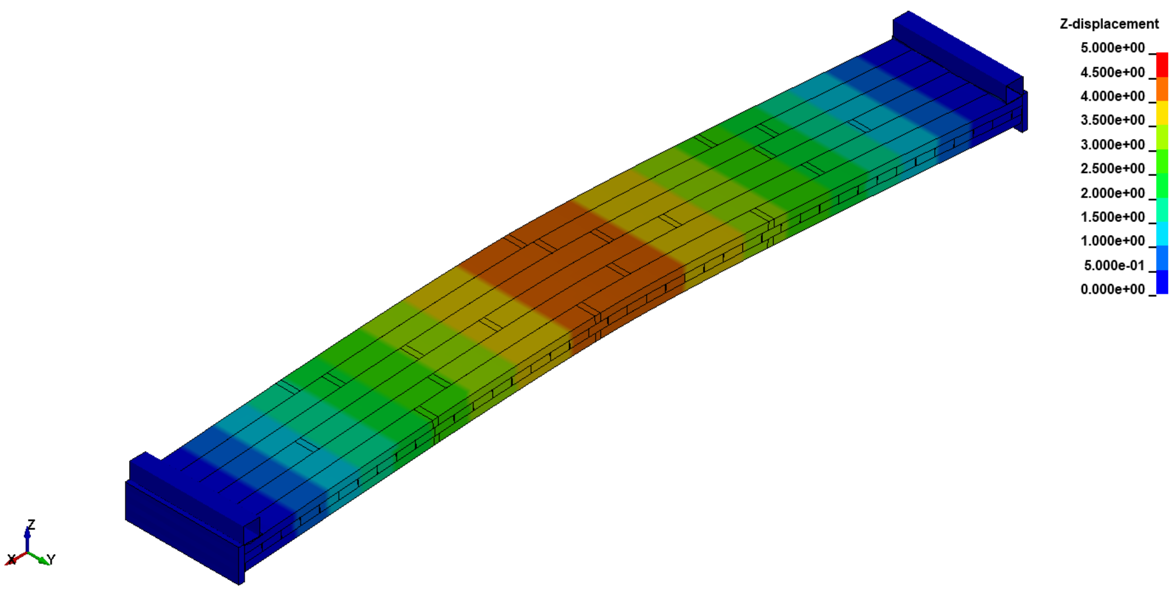


*(b) Simulation screenshot (resultant displacement in inches).*

**Figure 4-12. 3-Ply Grade V1 Panel Top Surface Comparison (40% $F_c^*$).**

The out-of-plane pressure versus displacement results for the panels recorded in the tests and computed via the HFPB models are shown in Figure 4-13. Additionally, two reference lines pertaining to idealized boundary conditions (i.e., S-S: simple-simple; F-F: fixed-fixed) assuming elastic panel response are included. The following observations are made:

- The computed initial stiffness matches the measured (test) initial stiffness well for all axial loads simulated.

- Although the peak out-of-plane resistance of the panel is computed, the panel does not rupture on its top surface for the 20% $F_c^*$, 30% $F_c^*$, and 40% $F_c^*$ axial load cases.

- The peak out-of-plane resistance is markedly underpredicted by the HFPB model.

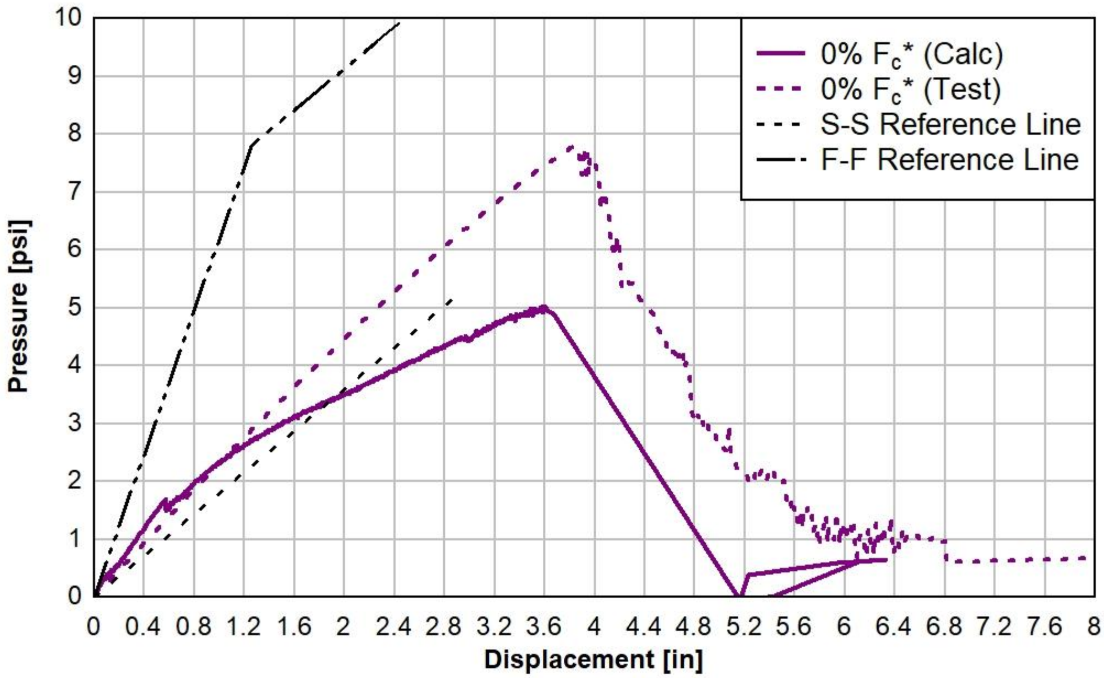


*(a) 0% $F_c^*$.*

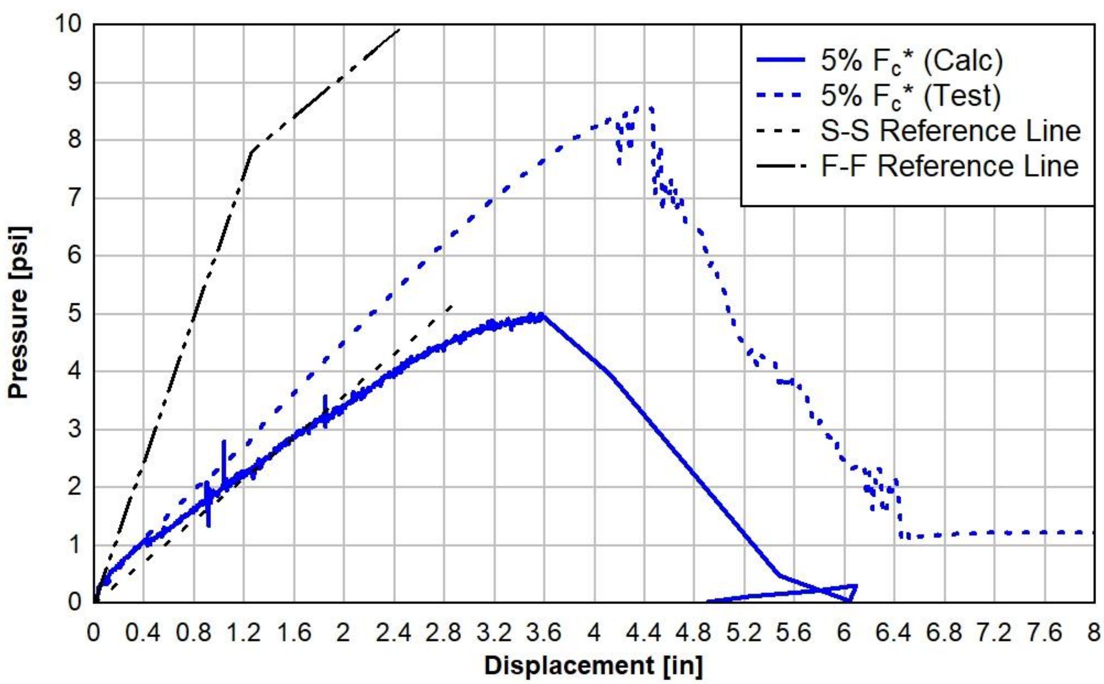


*(b) 5% $F_c^*$.*

**Figure 4-13. Comparisons of Out-of-Plane Resistance of Axially-Loaded CLT Panels.**

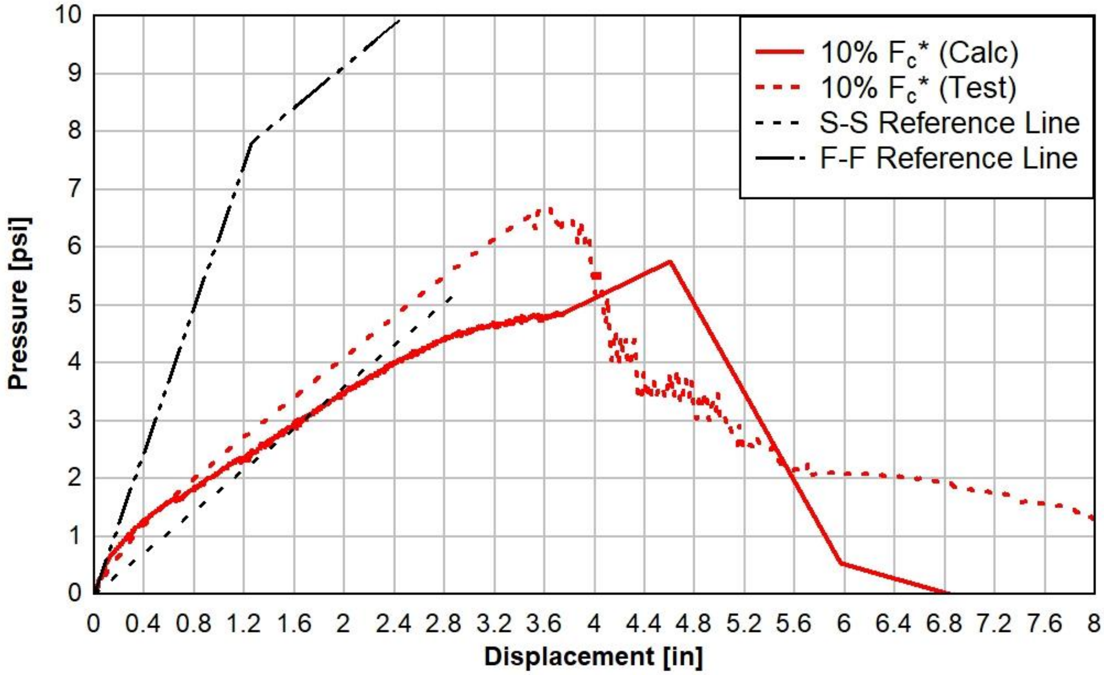


*(c) 10% $F_c^*$.*

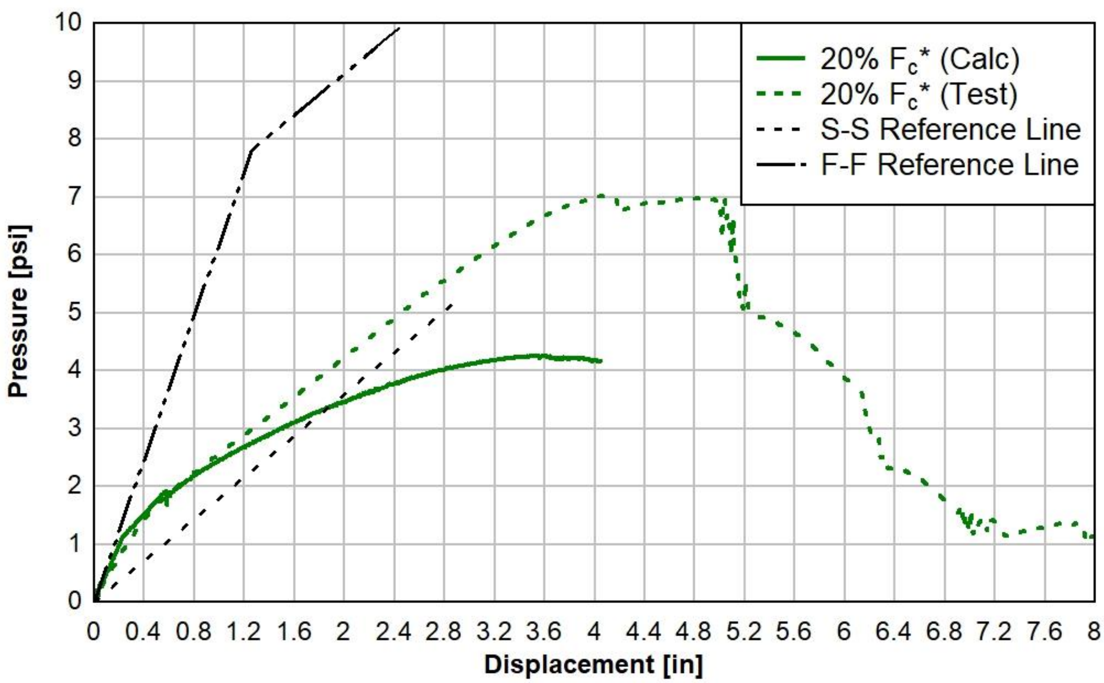


*(d) 20% $F_c^*$.*

**Figure 4-13. Comparisons of Out-of-Plane Resistance of Axially-Loaded CLT Panels. (Cont'd)**

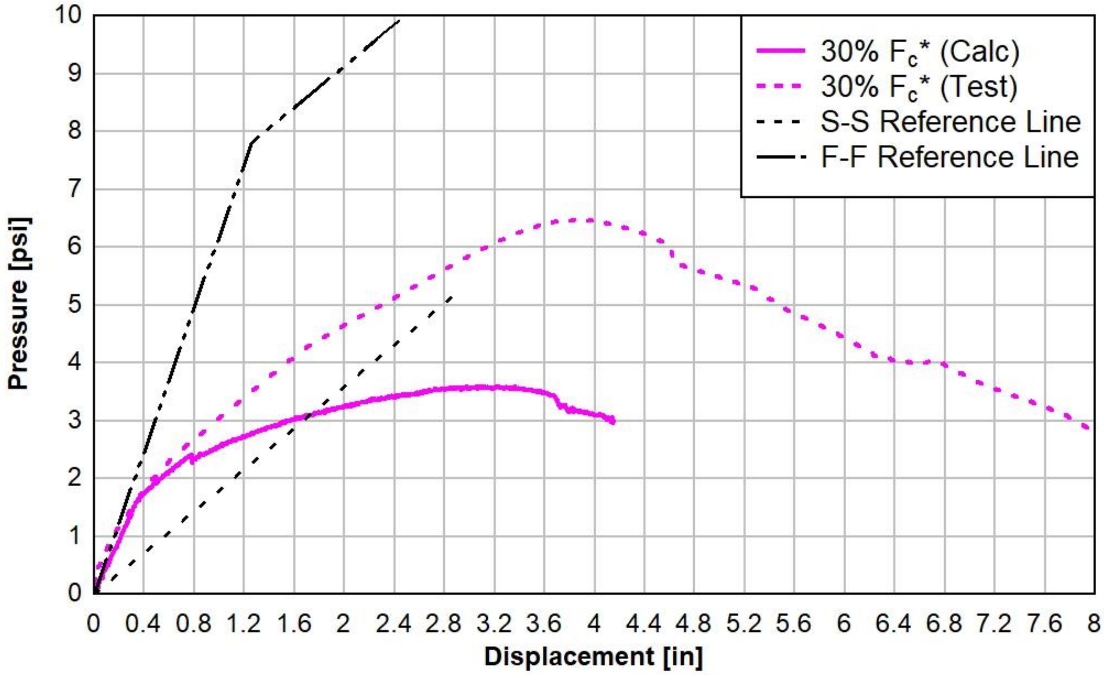


*(e) 30% $F_c^*$.*

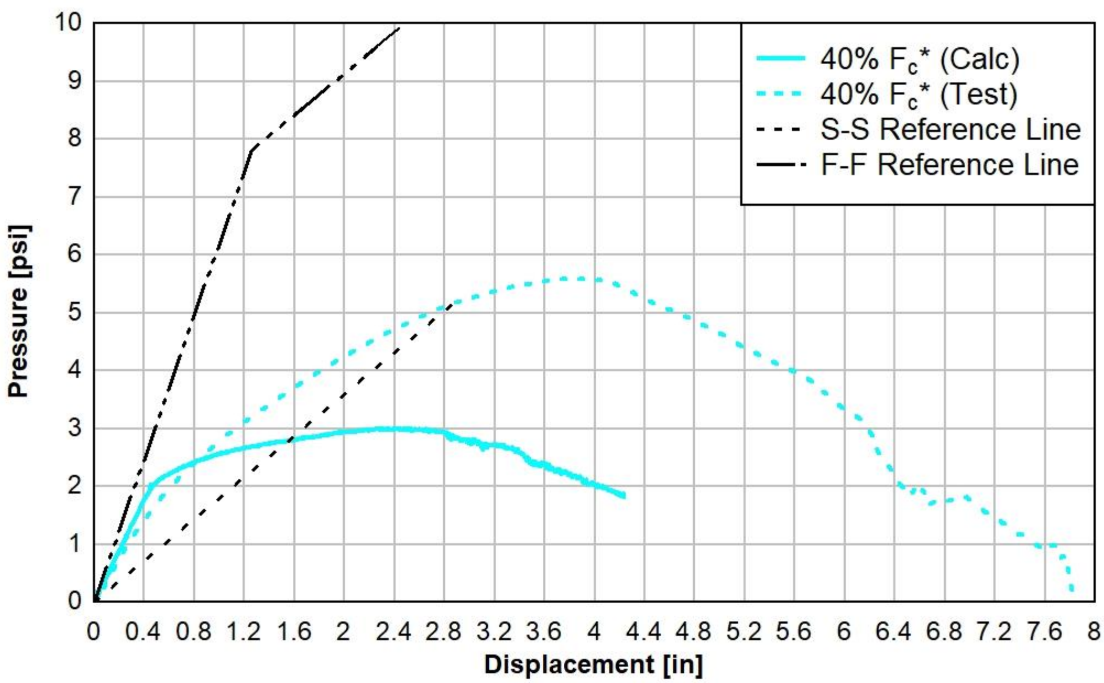


*(f) 40% $F_c^*$.*

**Figure 4-13. Comparisons of Out-of-Plane Resistance of Axially-Loaded CLT Panels. (Cont'd)**

# CHAPTER 5

# STRUCTURE BLAST TESTING CALCULATIONS

This chapter describes a series of analyses performed to evaluate an HFPB model's capability to predict the results from blast tests performed at Tyndall Air Force Base (AFB). The primary purpose of these calculations was to assess the ability of MAT_143 to reproduce structure responses under dynamic loads. The material model fits are described in Chapter 2 and the HFPB CLT panel models are consistent with those described in Chapter 3, albeit now for much larger structures.

The Tyndall AFB blast tests that are modeled are briefly described in Section 5.1. Details pertaining to the HFPB model, boundary conditions, and blast loading are given in Section 5.2. The results obtained from these simulations are shown in Section 5.3.

## 5.1 BLAST TESTING OVERVIEW

A series of blast tests was performed on three two-story, single-bay (i.e., roughly 15-foot square) CLT structures at Tyndall AFB. Each structure was constructed using a different grade of CLT (i.e., Grades V1, E1, and V4) and included window and door openings on their side walls consistent with an actual building. Two structures (i.e., Grades V1 and E1) had roughly 12-foot story heights and one structure (i.e., Grade V4) had roughly 10-foot story heights. Self-tapping screws STS) and adhesive anchors were utilized with steel angles to connect the constituent panels of each structure to each other and a concrete foundation. The test articles are shown in Figure 5-1.

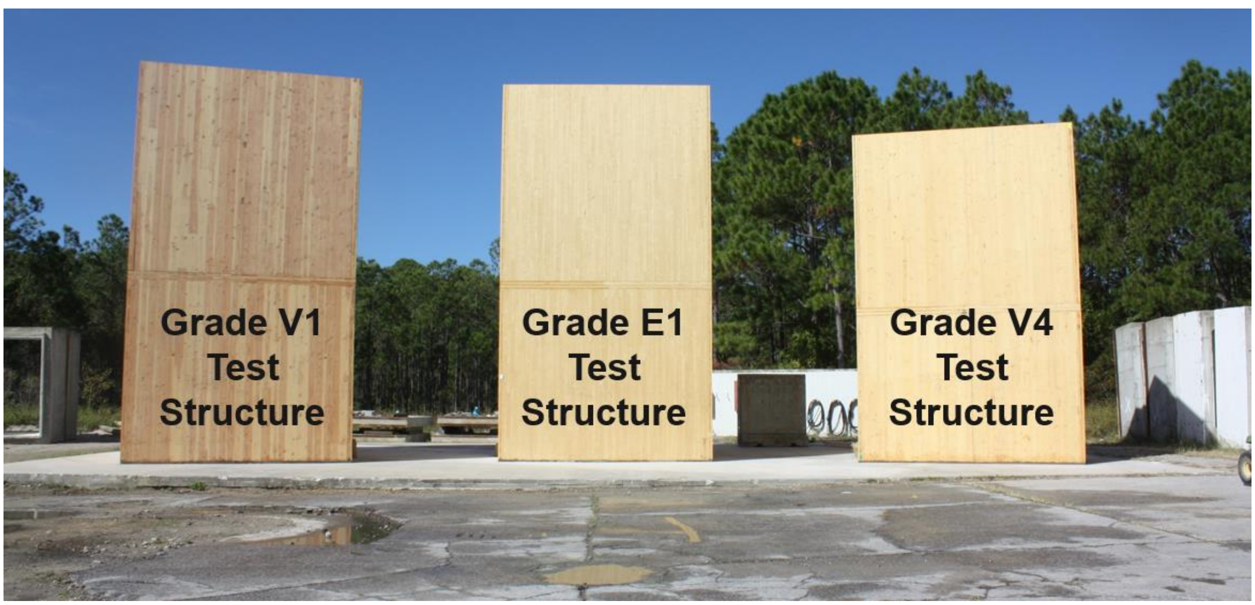


**Figure 5-1. Pre-Test Photograph of Front Walls of Test Structures.**

A total of seven blast tests were performed to demonstrate the effectiveness of CLT over a spectrum of blast loads. Tests 1 through 3 were performed during Phase 1 and Tests 4 through 7 were performed during Phase 2. For all tests, the standoff distance was held constant at 75 feet and the charge size was varied. Four tests were designed to keep the CLT panels within their elastic limits (i.e., Tests 1, 2, 4, and 6), three tests were designed to rupture the CLT panels (i.e., Tests 3, 5, and 7), and two tests were designed to investigate the response of axially-loaded panels (i.e., Tests 4 and 5). Ruptured panels were removed and replaced prior to the next test.

The Grade E1 structure for Tests 2, 3, and 7 were modeled as part of this effort. These tests are representative of the blast loads applied to the test structures and of the resulting front wall damage incurred. The roof and wall panels were 3-ply panels and the first elevated floor were constructed using 5-ply panels. Table 5-1 summarizes pertinent data related to these tests. Additional information concerning these tests can be found in [2] and [3].

**Table 5-1. Information Concerning Blast Tests Modeled.**

| Test | TNT Charge Size [lb] | Test Design Intent | Grade E1 Structure Front Wall Damage |
|---|---|---|---|
| 2 | 67 | To displace the 3-ply first-floor front panels of the Grade E1 test structure to its elastic limit displacement. | No observable damage. |
| 3 | 199 | To displace the 3-ply first-floor front panels of the Grade E1 test structure to 1.5 times its elastic limit displacement. | Plies on exterior and interior surface of first floor front wall ruptured near midspan. |
| 7 | 610 | To displace the 5-ply first-floor front panels of the Grade V1 test structure to 1.5 times its elastic limit displacement. | Front wall completely ruptured through at midspan at first and second levels. |

## 5.2 STRUCTURE HFPB MODEL

The HFPB model of the Grade E1 test structure described in the previous section is shown in Figure 5-2. A half-symmetry model of the structure was created to reduce run time. The model was constructed using panels identical in makeup to the UMaine panels described in Chapter 3. Additionally, the modeling decisions concerning element type (i.e., selective reduced integrated) and mesh size (i.e., 1-inch square with 3 elements through the thickness of each ply) were the same as those used in the calculations of the UMaine tests.

The geometry of the model faithfully reproduced the geometry of the actual test structure. These structures were not loaded with a superimposed load and gravity body forces were not included in the model. Modeling decisions concerning boundary conditions, hardware (e.g., self-tapping screws) modeling, and blast load application are discussed in the subsections that follow.

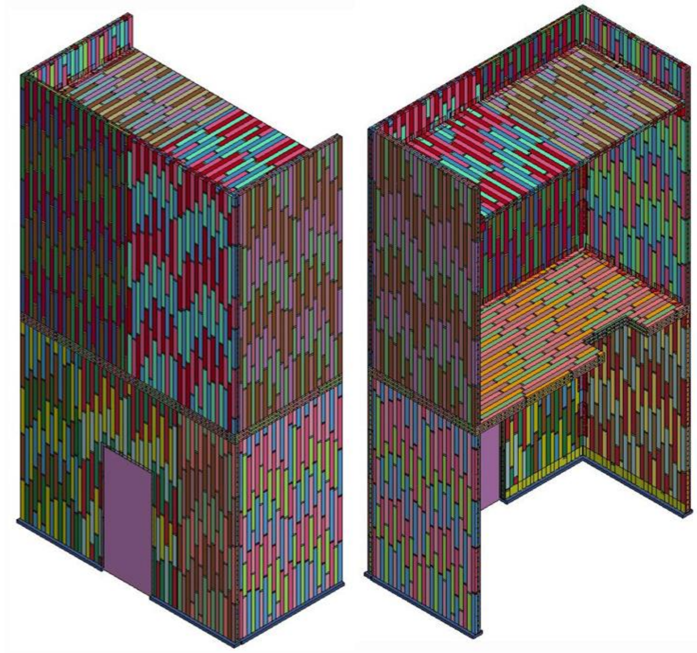

**Figure 5-2. HFPB Model of Grade E1 Test Structure (Half-Symmetry).**

### *5.2.1 Boundary Conditions*

Two types of boundary conditions were utilized for the HFPB model of the Grade E1 CLT test structure:

- Boundary condition at the bottom of the CLT structure. A layer of elastic concrete solid elements was used to simulate the contact surface of the structure with the slab on ground supporting it. The nodes on the bottom surface of these solid elements were restrained in all three translational degrees of freedom. This foundation concrete and the restrained nodes are shown in Figure 5-3a.

- A half symmetry boundary condition is applied to all nodes at the half symmetry boundary. This boundary condition consists of restraining translation in the Y-direction and rotation about the X and Z axes. The nodes to which this boundary constraint is applied are shown in Figure 5-3b.

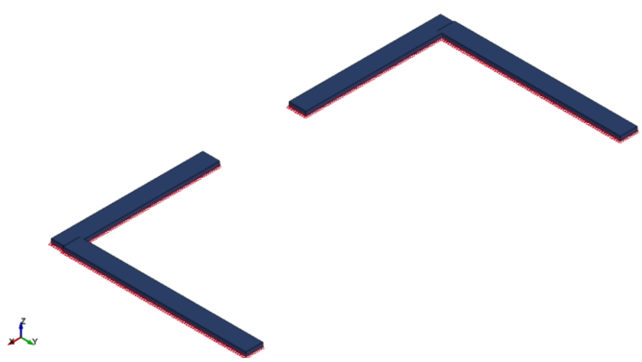

*(a) Foundation Concrete Boundary.*

**Figure 5-3. Test Structure Model Boundary Conditions.**

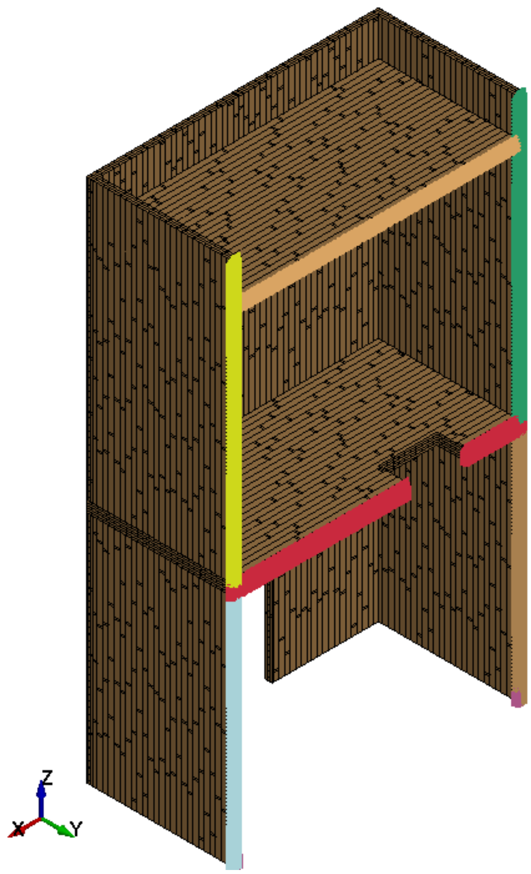


*(b) Half-Symmetry Boundary.*

**Figure 5-3. Test Structure Model Boundary Conditions. (Cont'd)**

### *5.2.2 Hardware Modeling*

Several forms of mechanical connectors (i.e., hardware) was utilized in the test structure for connecting the structure to the foundation, panels to panels, and the door to the jamb.

- The foundation connection was modeled using Hughes-Liu shell elements with five through the thickness integration points for the L7x4x3/8 angle and elastic steel beam elements for the adhesive anchors and self-tapping screws (STS). Elastic steel shell elements acting as washers were merged to the beam end and tied to the foundation angle shells for connectivity. The portion of the beam element inside the CLT panel was tied to the CLT panel. A nonlinear piecewise linear plasticity material model was used to allow for nonlinear deformation of the foundation angle. Figure 5-4 shows how the foundation connection was modeled.

- The panel-to-panel connection was modeled using Hughes-Liu shell elements with five through the thickness integration points for the angles/straps and elastic steel beam elements for the STS. Elastic steel shell elements acting as washers were merged to beam ends and tied to the angle shells for connectivity. The portion of the beam element inside the CLT panel was tied to the CLT panel. A nonlinear piecewise linear plasticity material model was used to allow for nonlinear deformation of the angles and straps. Figure 5-5 shows how the typical panel-to-panel connection was modeled.

- The door was modeled as an elastic steel shell with a thickness of 1.75 inches. The density of the door steel was modified such that the weight of the modeled door would match that of what was installed (i.e., roughly 5.25 psf).

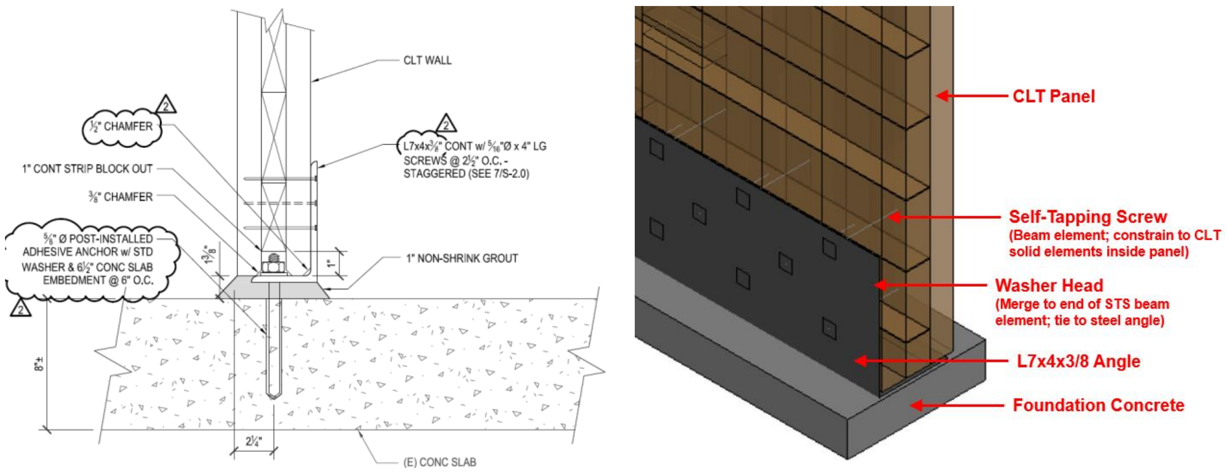


*(a) Detail.* *(b) HFPB Model.*

**Figure 5-4. Foundation Connection Model.**

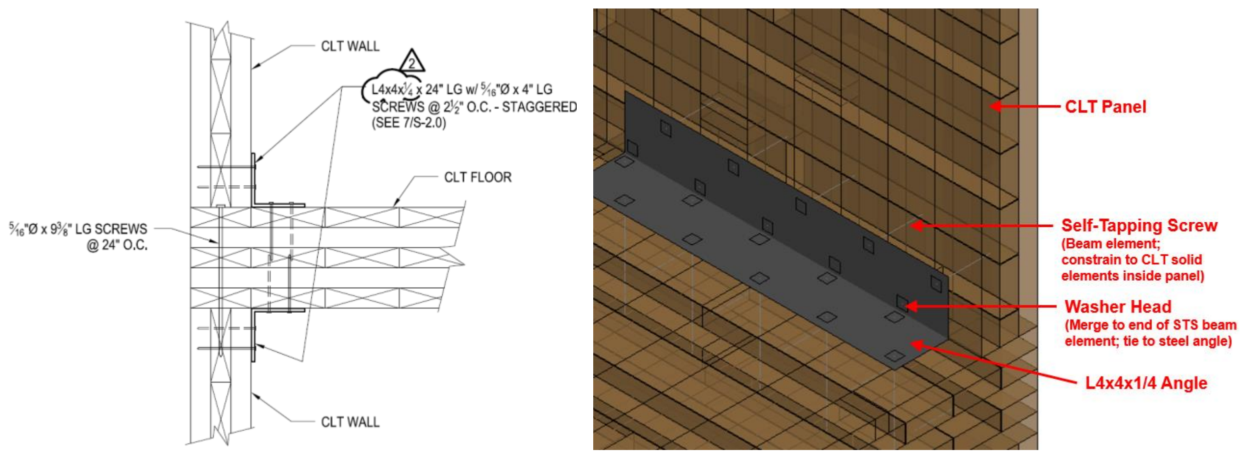


*(a) Detail.* *(b) HFPB Model.*

**Figure 5-5. Panel-to-Panel Connection Model.**

### 5.2.3 Rate Effects

As mentioned in Section 2.3.4, the default MAT_143 rate effects parameters were used for load durations of less than one second. This method of applying rate effects to CLT panels will be referred to as Strain Rate Method 1 (SR1). Another means to apply rate effects is to simply use a DIF of 2.0 in Equations (5) through (9) of Chapter 2 and turn rate effects off in the MAT_143 material card. This DIF value of 2.0 corresponds to the load duration factor, $C_D$, defined in the NDS for "impact" load durations [10]. This second method of applying rate effects to CLT panels will be referred to as Strain Rate Method 2 (SR2).

The impact of using SR1 and SR2 rate effects methods was performed based on the computed front wall displacements for Test 2. The computed displacements at three points on the front wall were measured and are plotted in Figure 5-6a; the locations of these points are shown in Figure 5-6b. For the smallest rate of applied loading (i.e., at Node 9150104), the relative difference between the SR1 and SR2 simulations is negligible. However, as the strain rate increases, the divergence between the SR1 and SR2 simulations also increases.

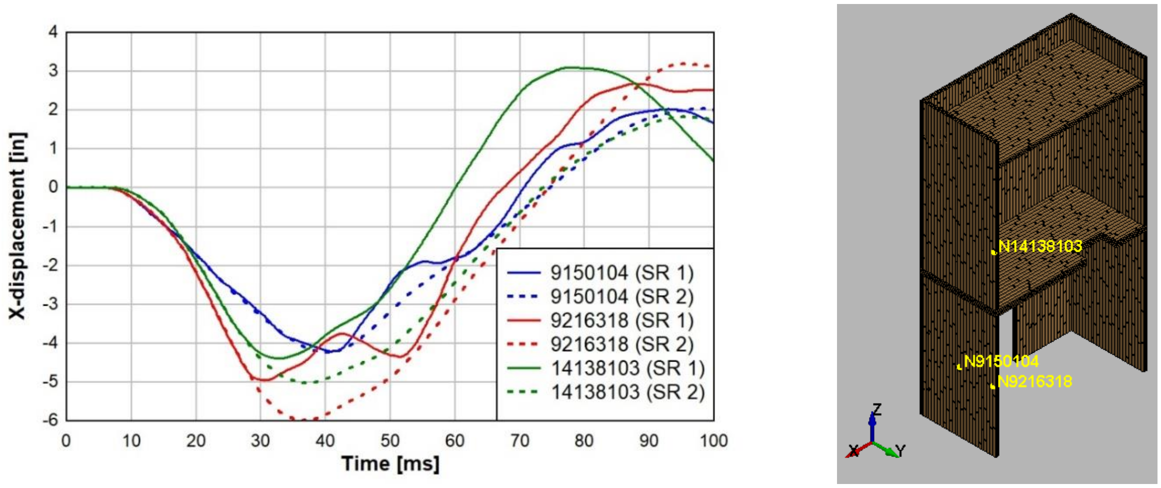


*(a) Computed displacement histories.* *(b) Node locations.*

**Figure 5-6. Rate Effects Study (Test 2 Front Wall Panels).**

For a model with many degrees of freedom, it is advantageous to have a means of automatically applying rate effects at the element, rather than the model, level. Thus, the SR1 method is used for the remaining simulations documented in this chapter.

## *5.2.4 Blast Load Application*

For these initial simulations investigating the ability of MAT_143 to reproduce dynamic CLT structural response, the "Load Blast Enhanced" (LBE) capability within LS-DYNA was used to generate blast loads. The LBE capability uses the Kingery-Bulmash (K-B) equations and the angle of incidence to generate blast loads at user-designated segments. For the far field blast loads of Tests 2, 3, and 7, this method will generate reasonably accurate blast loads with one caveat. Due to the small width of the structures (i.e., roughly 15 feet), the shock wave exhibited some clearing effects prior to the full reflected impulse being imparted to the structure. To address this issue, the charge sizes used in the simulations were reduced such that the positive phase impulses measured in the test and applied in the simulations were roughly equivalent. Table 5-2 documents the actual charge sizes used in the simulation.

**Table 5-2. Reduced Charge Sizes Used in Simulations to Account for Clearing Effects.**

| Test | Test Charge Size | Measured (Test) Blast Loads | Simulation Charge Size | Theoretical K-B Blast Loads |
|---|---|---|---|---|
| 2 | 67 | 7.94 psi / 32.9 psi-ms | 54 | 6.56 psi / 32.3 psi-ms |
| 3 | 199 | 13.2 psi / 65.2 psi-ms | 141 | 11.3 psi / 62.8 psi-ms |
| 7 | 610 | 27.0 psi / 134 psi-ms | 413 | 23.6 psi / 134 psi-ms |

Figure 5-7 compares the test data documented in Ref. [2, 3] (i.e., identified by gage number) with the LBE blast loads at the front wall of the Grade E1 structure. It is observed that although the peak pressures are routinely underpredicted by the LBE loads (as expected), the positive phase impulse matches well in all cases.

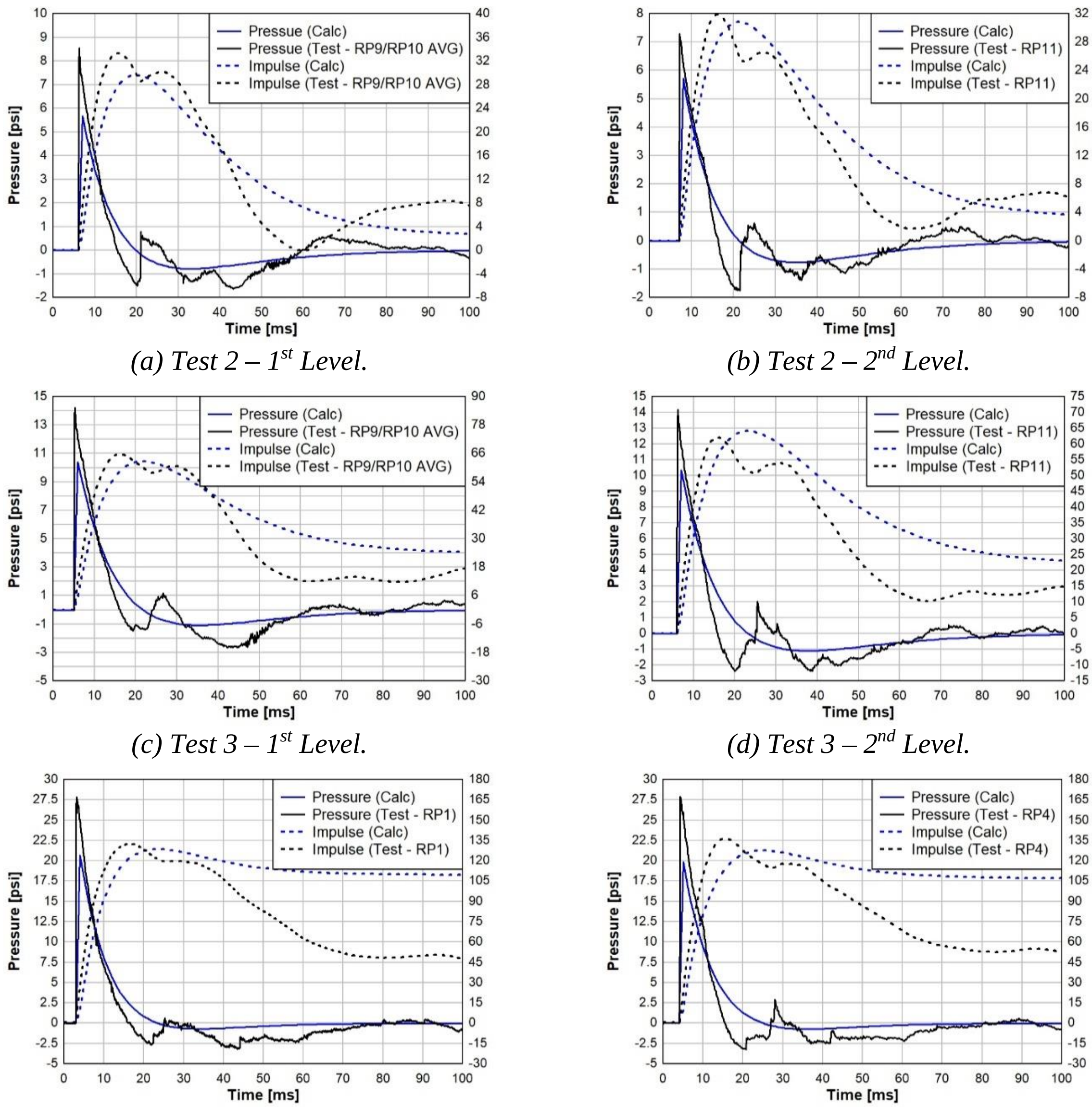


*(a) Test 2 – 1st Level.* *(b) Test 2 – 2nd Level.*

*(c) Test 3 – 1st Level.* *(d) Test 3 – 2nd Level.*

*(e) Test 7 – 1st Level.* *(f) Test 7 – 2nd Level.*

**Figure 5-7. Blast Load Test Versus Computed Comparisons.**

## 5.3 STRUCTURE HFPB RESULTS

Figure 5-8 includes screenshots showing the maximum inbound displaced response of the structures and the first-floor front panels. The focus of post-processing for these simulations is the front wall because this was structural damage was incurred. It is noteworthy that no element erosion at midspan occurs. In fact, upon reviewing the Z-stress data it appears that the interior face of the front wall panels does not generally reach the defined tension strength parallel to grain.

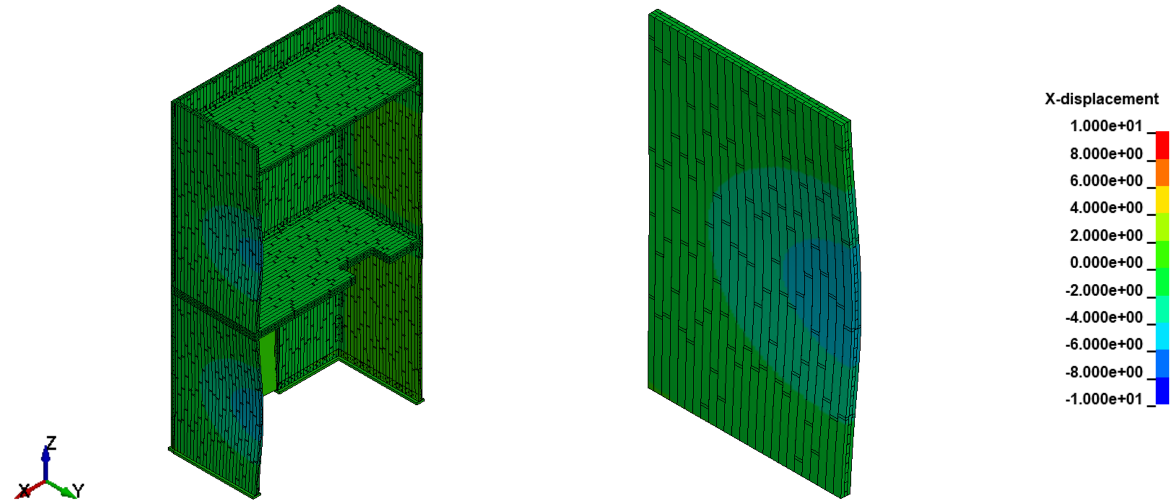


*(a) Test 2 – Full Structure.*　*(b) Test 2 – 1st Floor Front Wall.*

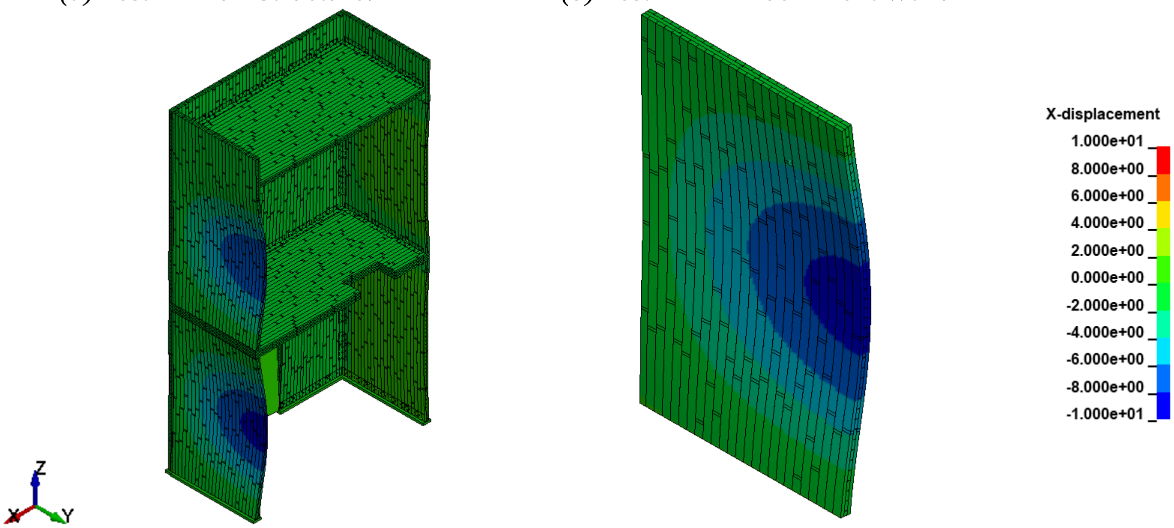


*(c) Test 3 – Full Structure.*　*(d) Test 3 – 1st Floor Front Wall.*

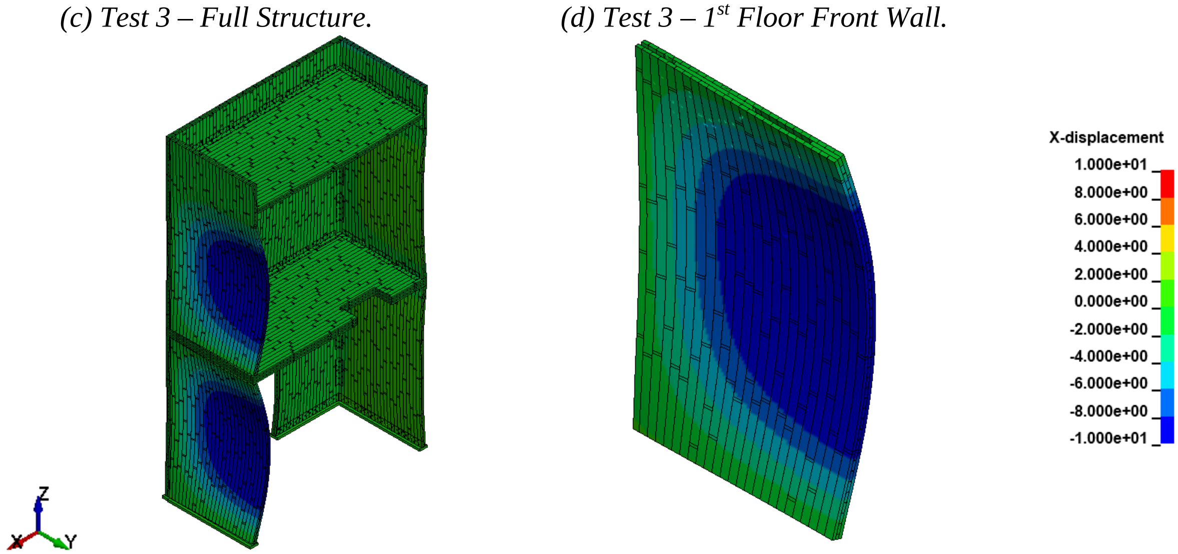


*(e) Test 7 – Full Structure.*　*(f) Test 7 – 1st Floor Front Wall.*

**Figure 5-8. Displacement Contours of Test Structure HFPB Model.**

*(X-displacement is in inches.)*

Figure 5-9 plots the X-displacement test data (as recorded by the gage in Ref. [2]) against the results of the simulations. No test data was available for Test 7. For both Tests 2 and 3, the measured (test) displacement data is significantly less than that predicted by the simulations.

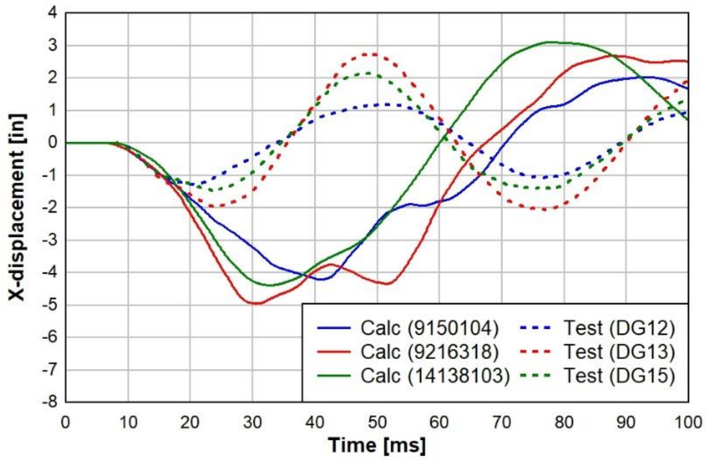


*(a) Test 2.*

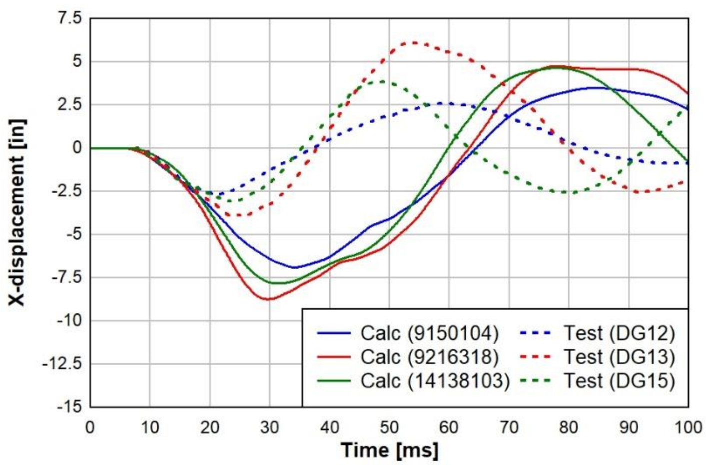


*(b) Test 3.*

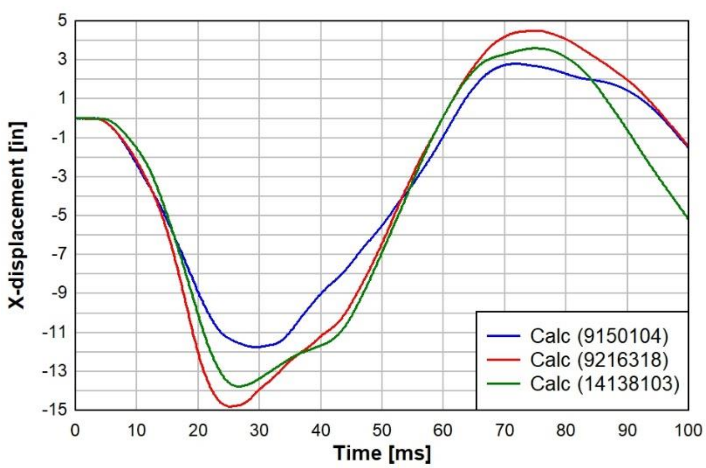


*(c) Test 7.*

**Figure 5-9. Test Structure Front Wall Displacement Comparison Plots.**

# CHAPTER 6

# CONCLUSIONS

## 6.1 SUMMARY

Following the conclusion of the quasi-static and blast testing of CLT panels documented in Ref. [1, 2, 3], a series of HFPB calculations were performed for some of these tests. The primary objective of these analyses was to assess the ability of a continuum FE approach to predict CLT panel responses up to and beyond panel rupture caused by quasi-static and dynamic (i.e., those associated with explosions) loads. Panel response both prior to and following rupture was considered. The model developed aimed to include the necessary fidelity to capture complex stress states explicitly while still being feasible from a computational cost perspective. Thus, a macroscale modeling approach was adopted.

Due to its anisotropic nature, wood is a difficult material to model in the HFPB context. An available material model developed by the FHWA (i.e., LS-DYNA's MAT_143) was utilized in this effort on account of its wood-centric focus. This material model uses transversely isotropic constitutive equations and the Modified Hanshin yield criterion to track and realize different post-peak behaviors characteristic of wood based on the state of stress. It also considers rate effects by increasing material strength with increasing strain rate.

Material model fits for the lumber constituting Grades E1, V1, and V4 CLT were derived based on the information provided in their respective APA product reports. A series of single element simulations were performed to test these fits in compression, tension, and shear force paths. In general, the simulations reproduced the input material properties. Several areas requiring further investigation were identified however:

- Beyond the proportional limit in compression, the material response is essentially plastic. No softening in the compression parallel to grain response is apparent even though softening has been reported in the literature.

- Elements appear to exhibit a significant amount of deformation capability in shear beyond the proportional limit, which is different than the data (albeit limited) documented in the literature.

- An anomalous result (Figure 2-12c) observed while performing mesh size sensitivity studies leads to questions concerning the robustness of the mesh regularization scheme.

- The strength increases associated with strain rates ranging from 0.05 to 5 $s^{-1}$ (i.e., common strain rates for structural components exposed to blast loads) appear to be excessively high and have no parallel to other materials documented in the literature.

Using the generated material model fits, CLT panels without axial load exposed to a uniformly-applied transverse quasi-static load in their major strength direction were modeled. To capture the observed failure at points of panel weakness (i.e., finger joints, knots), individual boards and finger joint locations were modeled. Sensitivity studies to ascertain optimal element type, mesh size, and loading rate were performed. The results of these simulations indicated that the generated material model fit reproduced the initial stiffness, peak strength, and residual capacity of the panels well.

Finally, quasi-static bending of biaxially-loaded CLT panels and dynamic bending of CLT panels were modelled using the material model fit and CLT panel modeling methodologies. These simulations uncovered several questions that suggest further investigation is required:

- The imposition of axial stress in combination with bending stress yielded computed peak panel strengths that were markedly less than those measured during testing. Thus, it is possible that the yield surface for biaxial stress states offered by MAT_143 is design conservative rather than predictive.

- Applying blast loads to CLT panels in an HFPB model led to markedly larger deflections than those measured in the test but also no panel rupture (or even attainment of their peak tension parallel to grain stress). This result is confusing, especially considering that the single element simulations did not intimate a decrease in material stiffness and that rupture was observed in quasi-static simulations for the same structural response (i.e., major strength direction bending).

## 6.2 NEXT STEPS

While the effort described herein uncovered several potential issues with MAT_143 in LS-DYNA, further material model development and validation efforts could be used to address these issues and unlock the power of first principles approaches for the wood community. The ability to effectively use continuum finite element methods to model CLT panels under complex quasi-static and dynamic load conditions would aid in the understanding of how CLT panels fail at both the panel and connection levels. The findings from such simulations could be used to refine current building code provisions and target future testing efforts. Additionally, the variability inherent in wood material properties could be explicitly addressed in the HFPB modeling paradigm through the use of various stochastic models.

The following actions represent steps to be pursued in light of the HFPB modeling approach and simulations documented herein:

- Further investigation into why the dynamic response of CLT panels is not well modeled by a CLT modeling approach that is notable for its efficacy at quasi-static loading rates merits attention.

- Expanding on (or redeveloping) the wood material model to address some of the limitations identified above. Chief among these would be the inclusion of compression softening for unconfined material, the refinement of fracture energy in shear, and more robust mesh regularization and rate effects schemes. A chief barrier to implementing these changes is the relative paucity of test data documenting the post-peak and high strain rate response of wood.

- Further investigation into yield surfaces that more directly represent the biaxial post-peak response phenomenology of wood would be of interest. Again, the paucity of test data in this space would need to be attended to.

- Wood is an inherently variable material. A deterministic approach to wood HFPB modeling is arguably flawed from the outset, although it is somewhat ameliorated in the case of macro-CLT response by the two-way action inherent in these panels. Scripts could be used to randomly assign different material cards to individual wood elements to explicitly account for this variability.

# APPENDIX A

# REFERENCES


[1] E. Nagy and M. K. Weaver, "Quasi-Static Out-of-Plane Testing of CLT and NLT Panels," Karagozian & Case, Inc., Glendale, CA, TR-16-42.1, 21 December 2016.

[2] M. K. Weaver, C. Newberry, C. O'Laughlin and L. Podesto, "Results from Blast Tests of Full-Scale Cross-Laminated Timber Structures," Karagozian & Case, Inc., Glendale, CA, TR-17-17.1, 27 September 2017.

[3] M. Weaver, C. Newberry, C. O'Laughlin and L. Podesto, "Results from Phase 2 Blast Tests of Full-Scale Cross-Laminated Timber Structures," Karagozian & Case, Inc., Glendale, CA, TR-18-06.2, 9 October 2020.

[4] "Wood Handbook - Wood an an Engineering Material," Forest Products Laboratory, Madison, WI, FPL-GTR-190, April 2010.

[5] S. Holmberg, K. Persson and H. Petersson, "Nonlinear Mechanical Behaviour and Analysis of Wood and Fibre Materials," *Computers and Structures,* vol. 72, no. 4-5, pp. 459-480, 1999.

[6] G. Eisenacher, R. Scheidemann, M. Neumann, B. Droste and H. Volzke, "Dynamic Crushing Characteristics of Spruce Wood Under Large Deformations," *Wood Science and Technology,* vol. 47, no. 2, pp. 369-380, 2013.

[7] A. Sretenovic, U. Muller and W. Gindl, "New Shear Assay for the Simultaneous Determination of Shear Strength and Shear Modulus in Solid Wood: Finite Element Modeling and Experimental Results," *Wood and Fiber Science,* vol. 36, no. 3, pp. 302-310, 2004.

[8] J. C. Xavier, N. M. Garrido, M. Oliveira, J. L. Morais, P. P. Camanho and F. Pierron, "A Comparison Between the Iosipescu and Off-Axis Shear Test Methods for the Characterization of Pinus Pinaster Ait," *Composites Part A: Applied Science and Manufacturing,* vol. 35, no. 7-8, pp. 827-840, 2004.

[9] C. C. Gerhards, "Effect of Duration and Rate of Loading on Strength of Wood and Wood-Based Materials," U.S. Forest Service, Forest Products Laboratory, Madison, WI, Report No. FSRP-FPL-283, 1977.

[10] "National Design Specification for Wood Construction," American Wood Council, Leesburg, VA, 2018.

[11] S. R. Reid and C. Peng, "Dynamic Uniaxial Crushing of Wood," *International Journal of Impact Engineering,* vol. 19, no. 5-6, pp. 531-570, 1997.

[12] A. Bragov and A. K. Lomunov, "Dynamic Properties of Some Wood Species," *Journal de Physique IV Colloque,* vol. 07, no. C3, pp. 487-492, 1997.

[13] J. A. Liska, "Effect of Rapid Loading on the Compressive and Flexural Strength of Wood," U.S. Forest Service, Forest Products Laboratory, Madison, WI, Report No. 1767, 1955.

[14] A. J. Panshin and C. de Zeeuw, Textbook of Wood Technology, New York, NY: McGraw-Hill Book Company, 1970.

[15] "LS-DYNA Keyword User's Manual, Release 10.0," Livermore Software Technology Corporation, Livermore, CA, October 16, 2017.

[16] Y. D. Murray, "Manual for LS-DYNA Wood Material Model 143," U.S. Department of Transportation, Federal Highway Administration, McLean, VA, Publication No. FHWA-HRT-04-097, August 2007.

[17] Y. D. Murray, J. D. Reid, R. K. Faller, B. W. Bielenberg and T. J. Paulsen, "Evaluation of LS-DYNA Wood Material Model 143," U.S. Department of Transportation, Federal Highway Administration, McLean, VA, Publication No. FHWA-HRT-04-096, August 2005.

[18] "APA Product Report: Nordic X-Lam, Nordic Structures," The Engineered Wood Association, PR-L306, 5 September 2018.

[19] "APA Product Report: SmartLam Cross-Laminated Timber, SmartLam, LLC," The Engineered Wood Association, PR-L319, 15 August 2018.

[20] "APA Product Report: DRJ Cross-Laminated Timber, D.R. Johnson Wood Innovations," The Engineered Wood Association, PR-L320, 4 September 2018.

[21] "APA Product Report: Structurlam CrossLam, Structurlam Mass Timber Corporation," The Engineered Wood Association, PR-L314, 23 July 2018.

[22] PDC-TR 18-02, "Analysis Guidance for Cross-Laminated Timber Construction Exposed to Airblast Loading," U.S. Army Corps of Engineers Protective Design Center, Omaha District, September 2018.

[23] ANSI/APA PRG-320-2018, "Standard for Performance-Rated Cross-Laminated Timber," APA - The Engineered Wood Association, Tacoma, WA, 2018.

[24] ASTM D2915-17, "Standard Practice for Sampling and Data-Analysis for Structural Wood and Wood-Based Products," ASTM International, West Conshohocken, PA, 2017.

[25] "National Design Specification Supplement: Design Values for Wood Construction," American Wood Council, Leesburg, VA, 2018.

[26] D. P. Flanagan and T. Belytschko, "A Uniform Strain Hexahedron and Quadrilateral with Orthogonal Hourglass Control," *International Journal for Numerical Methods in Engineering*, vol. 17, no. 5, pp. 679-706, May 1981.

[27] R. W. Jokerst, "Finger-Jointed Wood Products," Forest Products Laboratory, Madison, WI, FSRP-FPL-382, April 1981.